# Unification of Finite Symmetries in Simulation of Many-body Systems on Quantum Computers

Victor M. Bastidas [1, 2, *] Nathan Fitzpatrick [3, *] K. J. Joven [2] Zane M. Rossi [4]
Shariful Islam [5] Troy Van Voorhis [1] Isaac L. Chuang [4, 6] and Yuan Liu [7, 8, 5, †]

[1] Department of Chemistry, Massachusetts Institute of Technology, Cambridge, MA 02139, USA
[2] Physics and Informatics Laboratory, NTT Research, Inc., 940 Stewart Dr., Sunnyvale, California, 94085, USA
[3] Quantinuum, Terrington House, 13-15 Hills Road, Cambridge CB2 1NL, United Kingdom
[4] Department of Physics, Massachusetts Institute of Technology, Cambridge, MA 02139, USA
[5] Department of Physics, North Carolina State University, Raleigh, NC 27606, USA
[6] Department of Electrical Engineering and Computer Science,
Massachusetts Institute of Technology, Cambridge, MA 02139, USA
[7] Department of Electrical and Computer Engineering,
North Carolina State University, Raleigh, NC 27606, USA
[8] Department of Computer Science, North Carolina State University, Raleigh, NC 27606, USA

Symmetry is fundamental in the description and simulation of quantum systems. Leveraging symmetries in classical simulations of many-body quantum systems often results in an exponential overhead due to the exponentially growing size of some symmetry groups as the number of particles increases. Quantum computers hold the promise of achieving exponential speedup in simulating quantum many-body systems; however, a general method for utilizing symmetries in quantum simulations has not yet been established. In this work, we present a unified framework for incorporating symmetry groups into the simulation of many-body systems on quantum computers. The core of our approach lies in the development of efficient quantum circuits for symmetry-adapted projection onto irreducible representations of a group or pairs of commuting groups. We provide resource estimations for common groups, including the cyclic and permutation groups. Our algorithms demonstrate the capability to prepare coherent superpositions of symmetry-adapted states and to perform quantum evolution across a wide range of models in condensed matter physics and *ab initio* electronic structure in quantum chemistry. Specifically, we execute a symmetry-adapted quantum subroutine for small molecules in first quantization on noisy hardware, and demonstrate the emulation of symmetry-adapted quantum phase estimation for preparing coherent superpositions of quantum states in various irreps of a symmetry group. In addition, we present a discussion of major open problems regarding the use of symmetries in digital quantum simulations of many-body systems, paving the way for future systematic investigations into leveraging symmetries for practical quantum advantage. The broad applicability and rigorous resource estimation for symmetry transformations make our framework appealing for achieving provable quantum advantage on fault-tolerant quantum computers. The efficiency of the proposed symmetry-adapted subroutine holds the promise for exponential speedup in quantum simulation of many-body systems for symmetry-related properties.

## I. INTRODUCTION

Symmetry is an important concept and it has been widely used in many fields, ranging from unification of fundamental interactions in physics [1, 2] and the foundation of complexity theory in computer science [3, 4], to the description of materials and molecules [5, 6].

To formally describe symmetries, sophisticated mathematical tools such as group and representation theory have been developed [7, 8]. These tools include the transformation between group elements and their irreducible representations (irreps), i.e., the group Fourier transform, which conveniently captures this relationship [9, 10]. The group Fourier transform has found various application ranging from engineering to physical sciences [11]. In addition to individual groups, interesting

relationships between pairs of groups have been revealed, often called dualities [12, 13] which enable natural and simple decomposition for group actions and their representations. These group duality theorems result in powerful transformations between group elements and their irreps for pairs of commuting groups [14]. One prominent example is the Schur transform, which concerns the permutation and local unitary group pair [15].

These mathematical triumphs in group theory are accompanied closely by their powerful applications in the description [1, 2] and simulation [5, 6] of physical systems. For example, successful reduction in computational cost is routinely achieved in state-of-the-art classical simulation of quantum chemistry using point group symmetries [16] or periodic systems with translational symmetries [17]. Other quantum mechanical symmetries such as permutation of identical particles have also been considered [18]. In many-body systems, the spin of the particles is inherently related to their quantum statistics. In fact, fermions and bosons can be viewed as irreducible representations of the permutation group for

* These authors contributed equally to this work.
† Corresponding author: q_yuanliu@ncsu.edu

half-integer and integer spin, respectively [19]. In the fermionic case, examples of such symmetry include the construction of many-particle wave functions with a fixed total spin quantum number (or projection of total spin along a fixed axis), such as the spin-flip coupled-cluster theory [20, 21] and the celebrated unitary group approach (UGA) [22–26] and its variants [27].

However, leveraging group transformations beyond small physical systems has faced significant challenges. One major reason is that the size of underlying group (and the associated transformation) often scales *exponentially or combinatorially* with the number of particles in quantum systems. This leads to an exponential overhead to execute such transformations on classical computers.

Quantum information science provides novel tools and techniques to realize and make use of these powerful symmetry transformations. Not surprisingly, it has been discovered that *efficient* quantum circuits exist for some group Fourier transforms [28, 29] and the Schur transform [30, 31]. The group Fourier transform has been combined with controlled group actions to realize the so-called generalized quantum phase estimation algorithm [32, 33]. More recently, the Schur transform has been further generalized to include both the local unitary with its dual unitary, where efficient quantum circuits are developed for such mixed Schur transforms [34–36]. These quantum circuits for symmetry transformations [37] have been used in quantum information theory for testing states and channel properties [32, 38, 39] and for designing better quantum teleportation protocols [36].

Despite the progress on leveraging symmetry transformations in quantum information theory, utilization of symmetry transformations in quantum simulation remains rare. Scattered examples include symmetry-adapted hybrid quantum-classical algorithms to improve their performance [40, 41]. Symmetry is also used to protect certain quantum simulation algorithms [42–44]. A very similar approach to what is presented in this work has been applied to quantum machine learning of point cloud data [45].

As the description and analysis of many seemingly disparate quantum algorithms is simplified and made more uniform [46–48], a new opportunity has arisen in standardizing and simplifying the treatment of generic *symmetry-adapted* quantum subroutines. By doing so, one natural question becomes: is it possible to leverage the coherent nature of quantum computers to simultaneously produce a coherent superposition of states in different irreps of a symmetry group? If so, is it possible to achieve significant quantum speedup for a wide class of quantum simulation problems based on efficient quantum subroutines for symmetry transformation?

There are three key challenges for such a unified treatment of symmetry transformations for quantum simulation of physical systems. First, group theoretical transformations need to be converted into efficient quantum circuits, which are not obvious to achieve. Second, the quantum circuits developed for symmetry transforma-

tions often directly operate on qubits. It is not clear how to relate the qubit computational basis to degrees of freedom in physical systems of interest. This depends on how the underlying physical systems are mapped to quantum computers. Third, for different mappings, the intrinsic symmetry of the physical systems may manifest as different symmetries on quantum computers. For example, permutation symmetry of local fermionic operators becomes a non-local operation under the Jordan-Wigner transformation. This creates a gap between pure mathematical group representation theory and realistic many-body physical systems. It makes it even more challenging that this gap intertwines with the quest for *efficient* simulation of many-body systems using quantum algorithms.

In this work, we address these challenges by providing a general framework for leveraging arbitrary symmetry-adapted transformations to perform quantum simulation of many-body systems on quantum computers. As a second major contribution, we articulate open problems for provable quantum advantage in simulating many-body systems by exploiting symmetries. In more detail, we discuss efficient quantum circuit implementation of symmetry transformations for common groups and pairs of commuting groups relevant for many-body systems. We further demonstrate how such symmetry transformations can be used to transform physical states and operators on quantum computers.

We illustrate the broad applicability of our framework for symmetry-adapted preparation, Hamiltonian simulation and quantum phase estimation. Our methodology can be applied to diverse systems ranging from spin lattices in condensed matter physics to the *ab initio* electronic structure problem in quantum chemistry. Crucially, for a given many-body system, the symmetry-adapted transformation allows preparation and manipulation of coherent superposition of states within different irreps of a symmetry group on quantum computers. Circuit constructions and resource estimations are provided. Lastly, we validate our symmetry transformation subroutine by preparing coherent superposition of singlet and triplet states of $H_2$ molecules using a Noisy Intermediate-Scale Quantum (NISQ) device. We also demonstrate that the symmetry transform allows determination of singlet and triplet energies of $H_2$ simultaneously, which offers additional quantum speedups for chemistry simulations.

The rest of the paper is organized as follows. Sec. II provides constructions of quantum circuits for group Fourier transform and generalized phase estimation for single and pairs of commuting groups common in many-body systems. Sec. III discusses how to incorporate these symmetry routines in generic quantum algorithms to transform states and operators, with illustrative examples provided. We summarize major open problems in dealing with symmetries in many-body systems on quantum computers in Sec. IV. Conclusions and outlook are presented in Sec. V.

## II. SYMMETRY GROUP TRANSFORMS

We discuss symmetry group transformations and their quantum circuit realizations in this section. Sec. II A presents a general discussion on quantum character transforms and how they can be used to construct projections into particular irreps. Resource estimations on cyclic groups and symmetry groups are provided in Secs. II B and II C, respectively. The general case for finite groups is discussed in Sec. II D and direct product groups are discussed in Sec. II E.

### A. Quantum Character Transform and Group Symmetry Transformations

In this section, we will exploit the orthogonality relations of the characters of the irreps labeled by $\Gamma$ of a group $G$ to form quantum circuits for projection operators onto the subspace spanned by that irrep.

#### 1. Characters and Symmetry Projectors

The character $\chi_\Gamma(g)$ of a group element $g$ in the $\Gamma$-th irrep is the trace $\chi_\Gamma(g) = \sum_i D_{ii}^\Gamma(g)$ of the representation matrix $\boldsymbol{D}^\Gamma(g)$. The orthogonality relations for characters are

$$\frac{1}{|G|} \sum_{g \in G} \chi_\Gamma(g)\chi_{\Gamma'}^*(g) = \delta_{\Gamma,\Gamma'} , \tag{1}$$

where $|G|$ is the order of the group, $\delta_{\Gamma,\Gamma'}$ is the Kronecker delta, and $*$ denotes complex conjugation. Using this relation, the projection operator $\hat{P}^\Gamma$ into the $\Gamma$-th irrep can be derived using the characters of the group elements. The goal is to construct an operator that projects any quantum state $|\psi\rangle$ into the subspace according to the $\Gamma$-th irrep. The projection operator $\hat{P}^\Gamma$ for the $\Gamma$-th irrep can be defined as

$$\hat{P}^\Gamma = \frac{d_\Gamma}{|G|} \sum_{g \in G} \chi_\Gamma^*(g)\rho(g), \tag{2}$$

where $d_\Gamma$ is the dimension of the $\Gamma$-th irrep and $\rho(g)$ is a unitary operator representation acting on vector space $V$ corresponding to the group element $g$. Formally, $\rho : G \to \mathrm{GL}(V)$ is a mapping from a group $G$ to a general linear group on vector space $V$. To see how this works, the action of the projection operator on $|\psi\rangle$ is

$$\begin{aligned} \hat{P}^\Gamma |\psi\rangle &= \frac{d_\Gamma}{|G|} \sum_{g \in G} \chi_\Gamma^*(g)\rho(g) |\psi\rangle \\ &= a_\Gamma |\psi^\Gamma\rangle . \end{aligned} \tag{3}$$

Here, $a_\Gamma$ is the amplitude of the projection of $|\psi_\Gamma\rangle$ on $|\psi\rangle$ and $\rho(g)$ acts on the Hilbert space of $|\psi\rangle$. One can show

that $\hat{P}^\Gamma$ is indeed a projection operator and a proof is given in Appendix A.

Given a group $G$ and an element $g \in G$, the conjugacy class of $g$ in $G$ is the set $\mathcal{C}(g) = \{hgh^{-1} \mid h \in G\}$. From now on, we will label the conjugacy classes by $C$ to simplify the notation. In the case of abelian groups, all the irreps are one-dimensional, and the number of conjugacy classes equals the number of group elements, because all elements commute according to $hgh^{-1} = g$.

For groups with further structure where the conjugacy class has more than one elements, Eq. (3) can be factorized on conjugacy classes because *the characters of all group elements in the same conjugacy class are equal*

$$\hat{P}^\Gamma |\psi\rangle = \frac{d_\Gamma}{|G|} \sum_C^{N_{\mathrm{Conj}}} \chi_\Gamma^*(C) \left( \sum_{g \in C}^{|C|} \rho(g) |\psi\rangle \right) = a_\Gamma |\psi^\Gamma\rangle , \tag{4}$$

where $N_{\mathrm{Conj}}$ is the number of conjugacy classes while $|C|$ is the number of group elements in a given conjugacy class $C$. Here $\chi_\Gamma(C)$ denotes the character for a given conjugacy class $C$. Despite the similarity of Eq. (4) with (3), Eq. (4) has the advantage that this allows us to deal with only the irrep and conjugacy class label without the need to explicitly deal with each dimensions of an irrep (or similarly deal with each individual group element in the same conjugacy class). Applying a linear combination of projectors in Eq. (4) to a state $|\psi\rangle$, results in a superposition of states spanning each irrep $\Gamma$

$$\sum_\Gamma \hat{P}^\Gamma |\psi\rangle = \sum_\Gamma a_\Gamma |\psi^\Gamma\rangle , \tag{5}$$

which will allow coherent manipulation of all the irreps of a symmetry group simultaneously. In next section, we show how to achieve this on quantum computers by defining a new unitary transformation, the *Quantum Character Transform*.

#### 2. Quantum Character Transform and Group Symmetry Transformations

For a given group, the column index of the character table runs through conjugacy classes $C$ and the row index represent the irreps $\Gamma$. The number of conjugacy classes is equal to the number of distinct irreps [49], which means the character table is a square matrix. Each column of the character table encodes the characters $\chi_\Gamma(C)$ of a given conjugacy class $C$ in different irrep subspace $\Gamma$. Group theoretical results guarantee that any two columns of the character table are orthogonal. Similarly, any two rows of the character table are also orthogonal if the order of each conjugacy class is properly included

$$\sum_C^{N_{\mathrm{Conj}}} \frac{|C|}{|G|} \chi_\Gamma(C)\chi_{\Gamma'}^*(C) = \delta_{\Gamma,\Gamma'} , \tag{6}$$

which can be derived from Eq. (1) by using conjugacy classes [50].

The orthogonal relationship in Eq. (6) suggests that the character table can be represented as a unitary matrix (up to constant rescaling factors), which can therefore be realized on a quantum computer! In more detail, the *Quantum Character Transform* (QCT) for a group $G$, which we denote $QCT_G$, can be written explicitly as

$$QCT_G = \sum_C^{N_{\mathrm{Conj}}} \sum_\Gamma \frac{\sqrt{|C|} \cdot \chi_\Gamma(C)}{\sqrt{|G|}} |C\rangle \langle\Gamma| . \qquad (7)$$

As a result, the matrix elements of the QCT are given by the expression $QCT_{(C,\Gamma)} = \langle C| QCT_G |\Gamma\rangle = \frac{\sqrt{|C|} \cdot \chi_\Gamma(C)}{\sqrt{|G|}}$. As a familiar example, the quantum Fourier transform is nothing but the QCT for the cyclic group $\mathbb{Z}_N$ of $N$ elements $\{e, g, g^2, \cdots, g^{N-1}\}$. As $\mathbb{Z}_N$ is an Abelian group, the number of group elements equals the number of conjugacy classes.

The QCT can be combined with the following controlled group action to realize a quantum coherent superposition of all irrep sectors. Specifically, the controlled group action can be thought of as a SELECT operator indexed on the conjugacy classes, with all the group elements of the conjugacy classes controlled on the conjugacy class index $|C\rangle\langle C|$

$$\begin{aligned} \mathrm{SELECT}[\tilde\rho_G] &= \sum_C^{N_{\mathrm{Conj}}} |C\rangle\langle C| \otimes \frac{1}{|C|} \sum_{g\in C}^{|C|} \rho(g) \\ &= \sum_C^{N_{\mathrm{Conj}}} |C\rangle\langle C| \otimes \tilde\rho(C) , \end{aligned} \qquad (8)$$

where $N_{\mathrm{Conj}}$ is the number of conjugacy classes for the group of interest, and the conjugacy classes are iterated over in the summation. To simplify the notation, from now on we will drop the upper limit $N_{\mathrm{Conj}}$ of the sum over conjugacy classes. For convenience, we have defined $\tilde\rho(C) = \frac{1}{|C|} \sum_{g\in C}^{|C|} \rho(g)$, which is an equally-weighted Linear Combination of Unitaries (LCU), with each unitary being a unitary representation of the group element $g$. If $|C| > 1$, this can be implemented with a single additional PREPARE register when mid-circuit measurement and reset are used. This is shown in Sec. II D, with resource estimates for the general case.

Combining the QCT and the SELECT results in the Generalized Symmetry-Adapted Transform, $T_{\mathrm{GSA}}$. The abstract quantum circuit implementing $T_{\mathrm{GSA}}$ is shown in Fig. 1. The $T_{GSA}$ circuit acts on a quantum state
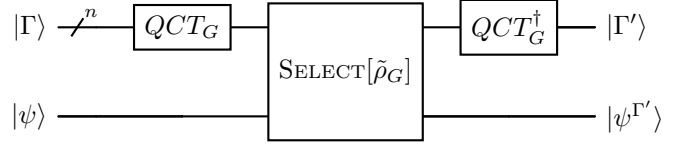


FIG. 1. Quantum circuit for $T_{\mathrm{GSA}}$ showing symmetry transformation circuits of $|\psi\rangle$ under irrep $\Gamma$, where $QCT_G$ is the quantum character transform as defined in Eq. (7). The square box is a multi-control that runs across all indexes on the $\Gamma$ register.

$|\Gamma\rangle \otimes |\psi\rangle$ as follows

$$\begin{aligned} T_{\mathrm{GSA}} |\Gamma\rangle \otimes |\psi\rangle &= \sum_{\Gamma'} \sum_C \frac{|C|}{|G|} \chi_\Gamma(C) \chi_{\Gamma'}^*(C) \tilde\rho(C) |\Gamma'\rangle \otimes |\psi\rangle \\ &= \sum_{\Gamma'} \frac{1}{|G|} \sum_C \chi_\Gamma(C) \chi_{\Gamma'}^*(C) \cdot \sum_{g\in C}^{|C|} \rho(g) |\Gamma'\rangle \otimes |\psi\rangle . \qquad (9) \end{aligned}$$

This circuit formulation slightly modifies Eq. (5). The character product can be expanded further using the Clebsch-Gordan relation $\chi_\Gamma(C)\chi_{\Gamma'}^*(C) = \sum_\lambda c_{\Gamma\Gamma'}^\lambda \chi_\lambda(C)$, $\forall C \in G$, where $c_{\Gamma\Gamma'}^\lambda$ are the Clebsch Gordan coefficients [50]. When $\Gamma = 0$ (the trivial representation), $\chi_0(C) = 1, \forall C \in G$. Eq. (9) simplifies to a rescaled a projector:

$$\begin{aligned} T_{\mathrm{GSA}} |0\rangle \otimes |\psi\rangle &= \sum_{\Gamma'} \frac{1}{|G|} \sum_C \chi_{\Gamma'}^*(C) \cdot \sum_{g\in C}^{|C|} |\Gamma'\rangle \otimes \rho(g) |\psi\rangle \\ &= \sum_{\Gamma'} \frac{1}{d_{\Gamma'}} |\Gamma'\rangle \otimes \hat P^{\Gamma'} |\psi\rangle \\ &= \sum_{\Gamma'} \frac{a_{\Gamma'}}{d_{\Gamma'}} |\Gamma'\rangle \otimes |\psi^{\Gamma'}\rangle , \qquad (10) \end{aligned}$$

where the post-selection probability to obtain a state in irrep $\Gamma'$ will be $|a_{\Gamma'}/d_{\Gamma'}|^2$, when the irrep register is measured. Therefore the $T_{\mathrm{GSA}}$ circuit rescales the projection by the dimension $d_\Gamma$ of the irrep $\Gamma$. If the input state on the ancilla register is a superposition of different irrep states, one should use $QCT_G^\dagger$. This can allow coherent control and simulation of states within individual irreps, where the number of required ancilla qubits to label a given irrep only scales logarithmically as the number of irreps increases. Such individual control on different irreps is desirable for applications such as quantum chemistry where a triplet electronic state will response differently to magnetic field than a singlet one, therefore may require different quantum subroutines to simulate. We leave further exploration of the advantages of $T_{GSA}$ in various applications to future works.

However, if the ancilla starts from $|0\rangle^{\otimes n}$ such as when using the $T_{\mathrm{GSA}}$ as a projector to a specific irrep $\Gamma$, a simpler PREPARE can be used as shown in Appendix B,

which can reduce the gate count significantly and also remove the $d_\Gamma$ by introducing a uniform renormalization factor. A similar circuit construction has been proposed in [45], with application to quantum machine learning.

To find the relevant symmetry transformation circuits, we require two fundamental operations: SELECT$[\tilde{\rho}_G]$ and $QCT$ for the relevant group. In particular, the controlled group actions and the $QCT$ are bespoke to each group arising from their structure. Some examples are presented in the next section.

## B. Cyclic Group $\mathbb{Z}_M$

In this section, let us consider a specific example of the QCT for the cyclic group $G = \mathbb{Z}_M$. This simplifies for the cyclic group as the group is abelian, and therefore, the number of group elements equals the number of conjugacy classes and $|C| = 1$. In this case, each irrep $\Gamma = k$ can be labelled using an integer $k = 0, 1, 2, \ldots, M-1$ (mod $M$) and is one dimensional $d_k = 1$ due to the abelian structure. Furthermore, $C = v$ will label the conjugacy classes. In our case, they are given by group elements $v = 0, 1, 2, \ldots, M-1$ $\chi_k(v) = e^{2\pi i k v/M}$ is the $k$th character of $\mathbb{Z}_M$ evaluated for $v$. The irreps of $Z_M$ are one-dimensional, and therefore, the irreducible representations can be defined in terms of the characters. The order of the group is $|G| = M$.

With all these elements at hand, from Eq. (7) we obtain the expression for the QCT for $G = \mathbb{Z}_M$

$$QCT_{\mathbb{Z}_M} = U_{\text{QFT}} = \frac{1}{\sqrt{M}} \sum_{k \in \mathbb{Z}_M} \sum_{v \in \mathbb{Z}_M} e^{2\pi i k v/M} |\boldsymbol{v}\rangle \langle \boldsymbol{k}| .$$
(11)

This expression is nothing but the quantum Fourier transform for a $m$-qubit system provided that $M = 2^m$ and by representing the group elements using the binary representation $\boldsymbol{v} = v_1 v_2 \cdots v_m$. More formally, the integer $v$ can be written as $v = v_1 2^{m-1} + v_2 2^{m-2} + v_m 2^0$. From now on, we will use $v$ to denote integers (mod $M$) while $\boldsymbol{v}$ will denote their binary representation.

One interesting example is the case $M = 2$, where the group Fourier transform acts on a single qubit and is given by a Hadamard gate $H$, as follows

$$QCT_{\mathbb{Z}_2} = H = \frac{1}{\sqrt{2}} \sum_{a=0}^{1} \sum_{b=0}^{1} (-1)^{ab} |a\rangle \langle b| .$$
(12)

The next step is to construct the controlled group action SELECT$[\tilde{\rho}_{\mathbb{Z}_M}]$. In the case of the cyclic group, the group elements $|\boldsymbol{v}\rangle = \hat{T}^v |\boldsymbol{0}\rangle = \bigotimes_{l=1}^{m} \hat{T}^{(v_l 2^{m-l})} |0_l\rangle$ appearing in Eq. (11) are generated by powers of the cyclic shift operator $\hat{T}$ such that $\hat{T}|\boldsymbol{j}\rangle = |\boldsymbol{j}+\boldsymbol{1}\rangle$ such that $\hat{T}^M = \hat{1}$ with $\hat{1}$ being the identity operation. When acting on the state representation spanned by $|\psi\rangle$, this
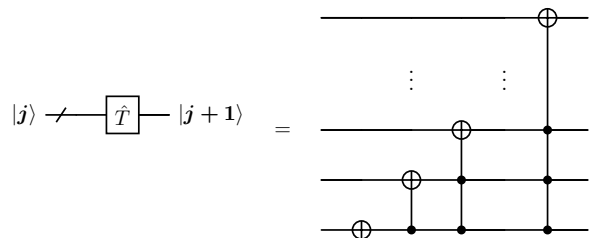


FIG. 2. Quantum circuit that increments an integer $\boldsymbol{j} = j_1 j_2 \cdots j_m$ by 1 to $\boldsymbol{j}+\boldsymbol{1}$, where each qubit on the right diagram represents a binary digit $j_l$ of $\boldsymbol{j}$. Here we use the binary decomposition $j = j_1 2^{m-1} + j_2 2^{m-2} + j_m 2^0$ of the integer $j$.

is the binary modular +1 increment operator. This is shown in Fig. 2. The controlled group action is a controlled indexed power of the same operator. The powers of $\hat{T}$ are simply implemented by sequential applications of the controlled circuit box. The factorization identity of Fig. 3 can, therefore, be used to reduce the number of multi-controlled operators

$$\text{SELECT}[\tilde{\rho}_{\mathbb{Z}_m}] = \sum_{v=0}^{M-1} |\boldsymbol{v}\rangle\langle\boldsymbol{v}| \otimes \hat{T}^v$$
(13)

$$= \prod_{l=1}^{m} \left[ |0\rangle\langle 0|_l \otimes I^{\otimes m} + |1\rangle\langle 1|_l \otimes \hat{T}^{2^{(m-l)}} \right] ,$$
(14)

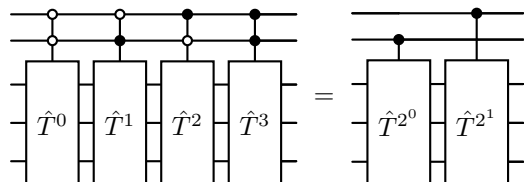where $v$ is the integer represented by the $m$-bit string $\boldsymbol{v}$ and $l$ labels the $l$th bit.



FIG. 3. Circuit identity for $\sum_{v=0}^{M-1} |\boldsymbol{v}\rangle\langle\boldsymbol{v}| \otimes \hat{T}^v$ showing how a linear combination of sequentially increasing powers of unitary $\hat{T}$ [51] can be efficiently factorized.

It is well known that the number of two-qubit gates in QFT scales as $O(m^2)$. For the cyclic group of $\mathbb{Z}_M$ there are $M$ irreps. Therefore, the irrep register which the QFT acts on, will have $m = \log_2(M)$ qubits. We assume this is a negligible cost and that the dominant cost is the powers of controlled increment boxes. This is displayed in Table I, where two compilation schemes are defined for the individually controlled group operation and the SELECT operation.

The naive compilation using the incrementer uses the compilation presented in Ref. [52], using $\log_2(m)$ conditionally clean qubits. The cost of the individual incrementation step is efficient; however, to apply the SELECT

| Primitive | Qubits | Ancilla | Controlled Increment$(+1)$ | | | SELECT | | |
|---|---|---|---|---|---|---|---|---|
| | | | T | Toffoli | Depth | T | Toffoli | Depth |
| Incremeter[52] | $m+1$ | $\log_2(m)$ | $12(m+1)$ | $3(m+1)$ | $O(m+1)$ | $O(\exp(m))$ | $O(\exp(m))$ | $O(\exp(m))$ |
| Adder [53] | $m$ | $m$ | $8m+O(1)$ | $4m$ | $O(m)$ | $8m^2+O(1)$ | $4m^2$ | $O(m^2)$ |

TABLE I. Resource estimates for two different implementations of the SELECT operation in the cyclic group projector and the controlled group action of a cyclic shift by binary increment $+1$ operation, for a cyclic group $\mathbb{Z}_M$ where $m = \log_2(M)$ is the number of ancilla qubits.
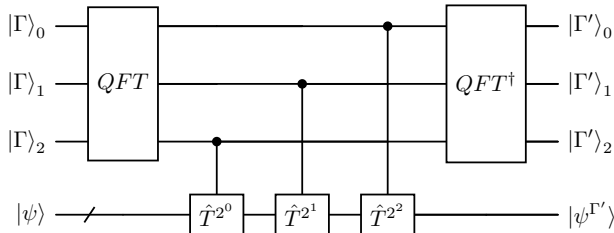


FIG. 4. Symmetry group transform quantum circuit for the cyclic group $\mathbb{Z}_8$.

operator, one must apply the controlled incrementer box $2^{m-1}$ times, as each $2^j$ controlled power requires $2^j$ individual sequential incrementation steps, which scales exponentially and is not suitable for large $m$. This can be improved using controlled addition circuits [53], at the cost of an extra $m$ qubits. This is because modular adders can be used to implement the cyclic shift, where each controlled power of the cyclic shift can be implemented by adding mod-$2^j$ via the initialization of the extra addition register at a cost independent from the size of the shift. Putting these all together, Fig. 4 displays an overall circuit for $T_{GSA}$ for the cyclic group $\mathbb{Z}_8$.

### C. Symmetric Group $S_N$

The Symmetric group is the group of $N!$ permutations of $N$ elements. The elements of the group can be represented in cycle notation. Each cycle can then be decomposed into a maximum of $N-1$ *transpositions*, where a *transposition* is a permutation of only two elements. There are $\frac{1}{2}[N(N-1)]$ unique transpositions which can generate the set of $N!$ permutations. Consider the permutation $g$ on the set $\{1, 2, 3, 4\}$ defined by $g = \begin{pmatrix} 1 & 2 & 3 & 4 \\ 2 & 3 & 4 & 1 \end{pmatrix}$. This permutation can be written in cycle notation as $g = (1\,2\,3\,4)$, which can be decomposed into a sequence of three transpositions $g = (1\,4)(1\,3)(1\,2)$. Hence, the controlled group actions in the SELECT can be formed as products of SWAP operations.

The conjugacy classes $\{C_j\}$ of the symmetric group are labelled by $\lambda$, a partition of $N$, $\lambda = (\lambda_1, \lambda_2, \ldots, \lambda_k)$ with $\lambda_1 + \lambda_2 + \cdots + \lambda_k = N$. For example, a permutation $g'$ of

the symmetric group of 5 elements $S_5$ can be expressed efficiently with the notation $g' \equiv (1, 3, 5)(2, 4)$. Such a permutation of a three-cycle and a two-cycle is said to have a $(3, 2)$ cycle structure, which is a partition of 5 elements. It is then readily seen that the conjugate of $g'$ by $g$ (for any $g \in S_5$) is the element $gg'g^{-1} = (g_1, g_3, g_5)(g_2, g_4)$, which has the same cycle structure as $g'$ and is therefore in the same conjugacy class. Hence, the conjugacy classes can be indexed by all possible cycle structures, which themselves can be labelled by partitions.

In addition to the conjugacy classes, the partitions $\lambda$ also label the irreps $\Gamma$, which can be shown through the use of Young symmetrisers and Young diagrams [49]. For small symmetric groups, the characters are tabulated, but one general formula for the corresponding irreducible character $\chi_\Gamma$ of $S_N$ can be expressed using the Frobenius character formula given in Appendix C.

As a simple example, the symmetry transformation circuits for $S_2$ can be constructed as follows. The group elements of $S_2$ are $\{e, (1, 2)\}$, where $e$ is the identity element. Thus, giving the group order of $|G| = 2$. In the circuit implementation the controlled group actions are simply an identity and a controlled swap gate on qubits 1 and 2. Here, the qubits are the objects being permuted. The characters of $S_2$ are well known as there are two irreps $\Gamma_1 = (2, 0) = \square\square$ (totally symmetric) and $\Gamma_2 = (1, 1) = \begin{array}{c}\square\\\square\end{array}$ (totally anti-symmetric). The characters are given by Table II

| | $e$ | $(12)$ |
|---|---|---|
| $\chi_{(2,0)}$ | 1 | 1 |
| $\chi_{(1,1)}$ | 1 | -1 |

TABLE II. Character table for the symmetric group $S_2$.

The Quantum Character Transform is therefore given by

$$QCT_{S_2} = \frac{1}{\sqrt{2}} \begin{bmatrix} 1 & 1 \\ 1 & -1 \end{bmatrix} = H, \tag{15}$$

which is a simple Hadamard gate formed from the normalized rows Table II. Putting this all together in circuit form, we obtain the symmetry-adapted transformation as depicted in Fig. 5.

In the general case of $S_N$ for $N > 2$, the symmetric group circuit for the QCT is more complicated due to the branching structure in the Bratelli diagram arising from
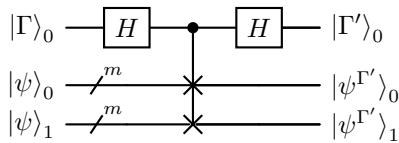
FIG. 5. $S_2$ symmetry projection circuit, acting on two system registers $|\Psi\rangle_0$ and $|\Psi\rangle_1$ of $m$ qubits each and one ancilla qubit $|\Gamma\rangle_0$. Comparing with Fig. 1, the $QCT$ is reduced to a Hadamard gate and the SELECT operation is implemented by an identity (no operation) and a controlled SWAP in the above. In this case, $T_{\text{GSA}}$ of the group $S_2$ reduces to the familiar SWAP test on the two system registers. This circuit can be used to project an arbitrary initial state on two system registers to their symmetric and anti-symmetric sectors.

the group subduction chain $S_N \supset S_{N-1} \supset \cdots \supset S_1$. For an efficient method to generate the QCT, a recursive method for the generation of characters based on this Bratelli diagram [54, 55] will need to be used, as the Bratelli diagram encodes a factorization of the internal subspaces. Possible candidates could be the Murnaghan–Nakayama rule or the more recent method proposed by Holmes [56]. However, an efficient circuit construction for the full Symmetric group Fourier transform is known as shown in D 1, from which it is known that the characters could be obtained from by tracing over the irreps and factorizing on the conjugacy class.

A possible method for the general construction of the SELECT primitive could use the fact that the symmetric group for $N!$ group elements can be factorized into $\frac{1}{2}(N(N-1))$ transpositions. A quantum circuit has been presented to generate the indexed set of $N!$ group elements from the transpositions using controlled SWAP gates by Laborde et al. [57]. However, it is unclear how this strategy could be combined with the methodology presented here, which needs to group the conjugacy classes containing $|C|$ group elements under a common index governed by the common cycle structure of the permutations. To form an efficient control structure indexed on the conjugacy classes generated from the group generators, one must know how the conjugacy classes are produced from the generators and encode that information as efficient quantum circuits.

### D. General Case for Finite Groups

As long as the group is finite, the group action on the space of $|\psi\rangle$ is known, and the quantum character transform can be formed, the approach presented in Fig. 1 can be used in general. In this section, some general strategies for constructing the QCT and the controlled group action will be presented.

#### 1. Quantum Character Transform

The QCT is a square matrix containing the normalized character table of the group and 1 on the rest of the diagonal for the indices greater than the number of conjugacy classes $N_{\text{Conj}}$. Often the character tables are known or can be calculated efficiently classically, scaling sub-exponentially with the size of the group. Even for the $O(N!)$ scaling symmetric group of $N$ elements, the number of conjugacy classes scales approximately: $\frac{1}{4N\sqrt{3}}\exp\left(\pi\sqrt{\frac{2N}{3}}\right)$ as $N \to \infty$ [49]. Therefore, it is not unquestionable that generating a QCT circuit could be achieved in a brute force manner by combining classically-generated character tables and recent algorithms such as the fast Hadamard transform[58]. However, it is likely that the optimal strategy is a recursive structure encoded into the circuit, such as generating the characters recursively from the branching of the subgroup chain of $S_N$ via the method of [56].

#### 2. SELECT Circuits

The quantum circuits for implementing the SELECT oracle applying the group actions grouped into their conjugacy classes acting on a state $|\psi\rangle$ indexed on a control register are presented in this section. The circuits implementing Eq.(8) are shown in Figs. 7 and 6. The sum over the conjugacy classes $\sum_j |C_j\rangle\langle C_j| \cdot \tilde{\rho}(C_j)$ is implemented by a series of multi-controlled operations which index the $N_{\text{Conj}}$ conjugacy classes on the register $|C_j\rangle$. This can be seen in Fig. 6 with a general formulation. Each $\tilde{\rho}(C_j) = \frac{1}{|C_j|}\sum_{g\in C_j}^{|C_j|} \rho(g)$ needs to be implemented as a nested Linear Combination of Unitaries (LCU) operation [59] to account for the action of all group elements in $C_j$. This is an equal superposition of group elements in the conjugacy class $C_j$. It is implemented with a state preparation unitary acting on the group element register where the state is encoded in the first column of the unitary

$$\text{PREP}\left(\frac{1}{\sqrt{|C|}}\right) = \sum_{g\in C} \frac{1}{\sqrt{|C|}}|g\rangle\langle 0| + \Pi_\perp = \begin{bmatrix} \frac{1}{\sqrt{|C|}} & \cdot & \cdots \\ \frac{1}{\sqrt{|C|}} & \cdot & \cdots \\ \vdots & \ddots & \cdots \\ \frac{1}{\sqrt{|C|}} & \cdot & \cdots \end{bmatrix}$$
(16)

where $\Pi_\perp$ is a projector to the orthogonal space spanned by the column vectors other than the first column, and we have dropped in the subscript $j$ in $C_j$ and use $C$, since (16) works for any conjugacy class. The same notation will be used in the following. This equal superposition can be implemented efficiently using the approach presented in Ref. [60]. Mid-circuit measurement and reset can be used, which will only ever result in the use of $\lceil\log_2(\max(C))\rceil$ extra ancilla qubits as shown in Fig. 7.
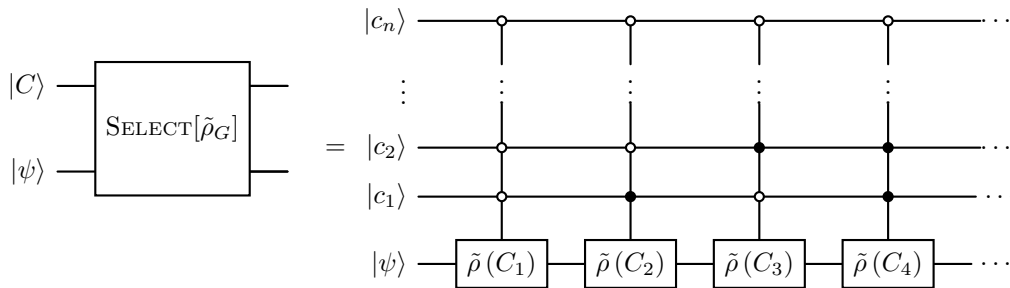
FIG. 6. SELECT circuit implementing $\sum_{j=1}^{N_{\text{Conj}}} |C_j\rangle\langle C_j| \cdot \tilde{\rho}(C_j)$ showing the first 4 terms of the controlled conjugacy classes of group actions acting on the space of $|\psi\rangle$ indexed on the conjugacy class $C_j$. The ancilla qubits are labeled as $|c_1\rangle, |c_2\rangle, \cdots, |c_n\rangle$, where $n = \lceil \log_2(N_{\text{Conj}}) \rceil$ for a bit representation $c_1 c_2 \cdots c_n$ of the integer $j$ labeling the conjugacy classes. $n$ is the number of qubits on the conjugacy class index register. $\tilde{\rho}(C_j)$ stands for the unitary operation on the system wave function $|\Psi\rangle$ corresponding to the $j$th conjugacy class $C_j$.
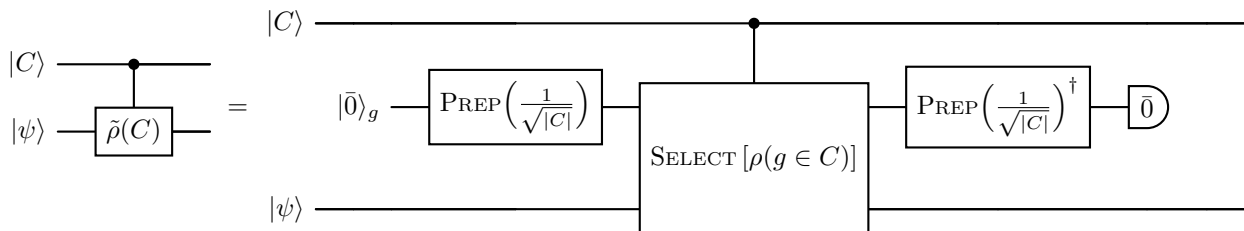


FIG. 7. Circuit showing the controlled LCU implementing $\tilde{\rho}(C) = \frac{1}{|C|} \sum_{g \in C}^{|C|} \rho(g)$ which is an equal superposition of representations of group elements within a conjugacy class $g \in C$. The equal superposition over $\frac{1}{|C|}$ is implemented via the two PREPARE oracles acting on the group element register $g$. The summation $\sum_{g \in C}^{|C|} \rho(g)$ is implemented by the SELECT oracle. Mid-circuit measurement, selecting the $\bar{0}$ results and reset of the group element register is used for efficient qubit count.

The nested SELECT operations can be implemented with unary iteration [60]. The upper bound of indexed operations is $D = N_{\text{Conj}} \cdot \max(|C|)$ with $O(4D - 4)$ $T$ gates, $O(D-1)$ Toffolis, at the addition of $O(\log(N_{\text{Conj}}) + \log(\max(|C|) - 1)$ ancilla qubits. $N_{\text{Conj}}$ is the number of conjugacy classes, and $\max(|C|)$ is the size of the largest conjugacy class. The SELECT operation, combined with the controlled group action $\rho(g)$ itself, is expected to be the dominant cost of the algorithm. This assumption can be made because the $QCT$ acts on $\lceil \log_2(\max(C)) \rceil$ qubits with the size of the conjugacy class known to scale sub exponentially even for the $N!$ scaling of the symmetric group $S_N$ [49]. To prepare the equal superposition across all conjugacy class elements, we require a linear number of qubits. The cost of the controlled group action will vary depending on the relevant group.

### E. Direct Product Groups

#### 1. General Discussion

Direct product groups is the mathematical tool for investigating physical systems containing multiple symmetries. In this section direct product of groups of the form $G \times G' = \{(g, g') \mid g \in G, g' \in G'\}$ will be implemented as a $T_{GSA}$. Each element of $G \times G'$ is a pair $(g, g')$ and the group operation on $G \times G'$ is defined component-wise, meaning if $(g_1, g_1')$ and $(g_2, g_2')$ are elements of $G \times G'$, their product is given by $(g_1, g_1') \cdot (g_2, g_2') = (g_1 \cdot g_2, g_1' \cdot g_2')$, where $\cdot$ denotes the respective group operations in $G$ and $G'$. As we are working with representations of these groups acting on finite Hilbert spaces, we can define their respective representations $\rho_G : G \to \text{GL}(V)$ and $\rho_{G'} : G' \to \text{GL}(W)$. The group $G \times G'$ therefore acts on the tensor product space $V \otimes W$ by $[\rho_G(g) \otimes \rho_{G'}(g')](v \otimes w) = \rho_G(g)(v) \otimes \rho_{G'}(g')(w)$, where $v \in V$, and $w \in W$.

As a first step to define the transformation $T_{\text{GSA}}$ for a direct product of groups, we need to consider $m = m_g + m_{g'}$ qubits in the quantum circuit of Fig. 8 to

encode the group elements $g \in G \times G'$. Due to the direct product structure of the group, the quantum character transform naturally factorizes as a tensor product of the individual character transforms

$$QCT_{G \times G'} = QCT_G \otimes QCT_{G'}. \quad (17)$$

The direct product of controlled group actions can be defined by

$$\text{SELECT}[\tilde{\rho}_G \cdot \tilde{\rho}_{G'}] := \left( \sum_{C_G} |C_G\rangle\langle C_G| \otimes \rho(C_G) \right)$$
$$\otimes \left( \sum_{C_{G'}} |C_{G'}\rangle\langle C_{G'}| \otimes \rho(C_{G'}) \right) . \quad (18)$$

As both the Fourier and controlled group action factorize, the symmetry adapted transformation takes the form $T_{GSA} = T_{GSA}^{(G)} \otimes T_{GSA}^{(G')}$. We are using the notation $\rho(C_G) = \frac{1}{|C_G|} \sum_{g \in C_G} \rho(g)$ and $\rho(C_{G'}) = \frac{1}{|C_{G'}|} \sum_{g' \in C_{G'}} \rho(g')$ as they are representations acting on the same space. Note that we use the notation $\tilde{\rho}_G \cdot \tilde{\rho}_{G'}$ in the argument of the select operation because $\rho(g)$ and $\rho(g')$ act on the same vector space containing $|\psi\rangle$ and cannot be represented as an explicit tensor product in a circuit implementation. Its action on a quantum state is given by

$$T_{GSA} |0,0\rangle \otimes |\psi\rangle = \sum_{\Gamma_G \Gamma_{G'}} |\Gamma_G, \Gamma_{G'}\rangle \otimes \frac{\hat{P}_G^{\Gamma_G} \hat{P}_{G'}^{\Gamma_{G'}}}{d_{\Gamma_G} d_{\Gamma_{G'}}} |\psi\rangle$$
$$= \sum_{\Gamma_G \Gamma_{G'}} \frac{a_{\Gamma_G}}{d_{\Gamma_G}} \frac{a_{\Gamma_{G'}}}{d_{\Gamma_{G'}}} |\Gamma_G, \Gamma_{G'}\rangle \otimes |\psi^{\Gamma_G \Gamma_{G'}}\rangle , \quad (19)$$

The abstract quantum circuit implementing $T_{GSA}$ circuit is shown in Fig. 8.

When working with multiple groups acting on the same vector space, their representations may not commute with each other $\rho_G(g)\rho_{G'}(g') \neq \rho_{G'}(g')\rho_G(g)$. Despite this non-commutativity, the products of their respective projectors still correctly project onto the subspaces corresponding to their irreps, $\hat{P}_{G'}^{\Gamma_{G'}} \hat{P}_G^{\Gamma_G} |\psi\rangle = \hat{P}_G^{\Gamma_G} \hat{P}_{G'}^{\Gamma_{G'}} |\psi\rangle = |\psi^{\Gamma_G}\rangle \cap |\psi^{\Gamma_{G'}}\rangle$, because this projects onto the intersection of two symmetric sup spaces spanning the irreps $\Gamma_G$ and $\Gamma_{G'}$

### 2. Example on $\mathbb{Z}_N \times \mathbb{Z}_2$

In the previous section we discussed the general framework of the symmetry-adapted transformation for direct products of groups. In this section, we will provide a concrete example for the direct product group $\mathbb{Z}_N \times \mathbb{Z}_2$.

For convenience, we will use a representation of the Hilbert state basis using binary strings of length $N$. From

now on, we will use $|\boldsymbol{x}\rangle$ such that $Z_l |\boldsymbol{x}\rangle = x_l |\boldsymbol{x}\rangle$ with $x = 0, 1, 2, \ldots 2^N - 1$ to denote the basis and its binary representation $\boldsymbol{x} = x_1 x_2 \cdots x_N$. Next, let us define the group elements of commuting pair of groups $G = \mathbb{Z}_N$ and $G' = \mathbb{Z}_2$. The representation $\rho(G) = \{\hat{1}, \hat{T}, \hat{T}^2, \ldots, \hat{T}^{N-1}\}$ is generated by powers of the operator $\hat{T}$ such that $\hat{T}^N = \hat{1}$. We work on a representation such that powers of the $\hat{T}$ act as binary circular increment shifts. For example, $\hat{T}^n |\boldsymbol{x}\rangle = |\boldsymbol{y}\rangle$ is a shift of the digit $x$ to the left giving $y = 2^n x$. Similarly, the representation $\rho(G') = \{\hat{1}, \hat{\Pi}\}$ is generated by powers of the operator $\hat{\Pi}$ satisfying $\hat{\Pi}^2 = \hat{1}$. Its action on the quantum state is defined as $\hat{\Pi} |\boldsymbol{x}\rangle = |\bar{\boldsymbol{x}}\rangle$, which is nothing but a binary NOT operation on each bit of $\boldsymbol{x}$.

As the group $\mathbb{Z}_N \times \mathbb{Z}_2$ has a direct product structure, the corresponding group quantum character transform $QCT_{G \times G'} = U_{\text{QFT}} \otimes H$ is nothing but a product of the quantum Fourier transformation $U_{\text{QFT}}$ associated to the group $\mathbb{Z}_N$ and a Hadamard gate $H$, being the group Fourier transform of $\mathbb{Z}_2$. In this case, the symmetry-adapted transformation reads

$$T_{\text{GSA}} = H U_{\text{QFT}}^{-1} \otimes \text{SELECT}[\tilde{\rho}_{\mathbb{Z}_N \times \mathbb{Z}_2}] \otimes U_{\text{QFT}} H , \quad (20)$$

with the controlled group action defined as $\text{SELECT}[\tilde{\rho}_{\mathbb{Z}_N} \otimes \tilde{\rho}_{\mathbb{Z}_2)}]$. In this example, $\rho(gg') = \rho_1(g) \otimes \rho_2(g')$ is a one-dimensional representation of the group element $n \otimes \mu \in \mathbb{Z}_N \otimes \mathbb{Z}_2$ acting as $\rho(gg')|\boldsymbol{x}\rangle = |\boldsymbol{y}'\rangle$ where $\boldsymbol{x} = x_1 x_2 \cdots x_N$, $\bar{\boldsymbol{x}} = \bar{x}_1 \bar{x}_2 \cdots \bar{x}_N$ and $\bar{x}_l = 1 - x_l$. We use $\boldsymbol{y}'$ to denote the binary representation of $y' = 2^n(\bar{x}_1 2^{m-1} + \bar{x}_2 2^{m-2} + \bar{x}_N 2^0)$.

With these elements at hand, we can calculate the explicit action of the symmetry-adapted transformation in Eq. (20)

$$T_{\text{GSA}} |0\rangle |\psi\rangle = \sum_{k \in \mathbb{Z}_N} \sum_{\sigma \in \mathbb{Z}_2} |\boldsymbol{k}, \sigma\rangle |\psi^{k,\sigma}\rangle , \quad (21)$$

where $k$ and $\sigma$ label the irreps of $\mathbb{Z}_N$ and $\mathbb{Z}_2$, respectively. The projection operator

$$\hat{P}^{k,\sigma} = \frac{1}{2N} \sum_{\mu \in \mathbb{Z}_2} \sum_{n \in \mathbb{Z}_N} (-1)^{\mu\sigma} e^{-\frac{2\pi i k n}{N}} \hat{T}^n \hat{\Pi}^\mu \quad (22)$$

defines the symmetry-adapted state $|\psi^{k,\sigma}\rangle = \hat{P}^{k,\sigma} |\psi\rangle$, to project our state into the irreps labelled by $k$ and $\sigma$. Importantly, as we discussed above in Eq (19), the projector itself factorizes as $\hat{P}^{k,\sigma} = \hat{R}_k \hat{Q}_\sigma$, where $\hat{Q}_\sigma = (\hat{1} + (-1)^\sigma \hat{\Pi})/2$ and $\hat{R}_k = 1/N \sum_{n \in \mathbb{Z}_N} e^{-\frac{2\pi i k n}{N}} \hat{T}^n$ are projection operators into the symmetric subspaces labelled by $\sigma$ and $k$. In Sec. III D, we will provide an example on how to use this representation of the transformation $T_{\text{GSA}}$ to select from fermionic and bosonic, singlet and triplet on a $H_2$ system.
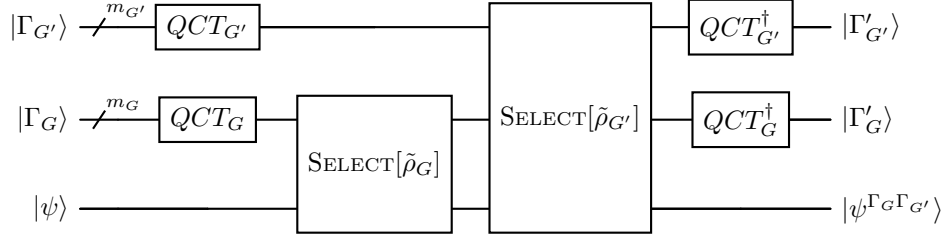
FIG. 8. Quantum circuit for $T'_{GSA}$ showing symmetry projection circuits of $|\psi\rangle$ onto the dual irrep $(\Gamma_G, \Gamma_{G'})$, where QCT is the quantum character transform as defined in Eq. (7). The $\text{SELECT}[\tilde{\rho}_{G'}]$ acts over the first and third wire only.

## III. EXAMPLES AND APPLICATIONS

So far, we have presented a framework for symmetry-adapted transformation for general groups. In this section, we provide concrete examples to illustrate the power of these unified symmetry-adapted transformations for quantum simulations. Sec. III A starts with an example of how to use the symmetry transformation with many standard quantum simulation routines such as the quantum phase estimation algorithm, to determine the spectrum of a many-body system when it is restricted to a given irrep of interest. Sec. III B discusses cyclic group with applications to a one-dimensional Ising model. Sec. III C expands consideration to a two-dimensional Harper-Hofstadter model with a pair of commuting cyclic groups. Sec. III D further expands the scope to three-dimensional *ab initio* quantum chemistry problems with permutation groups where $H_2$ is used as a specific example.

### A. Symmetry-Adapted Quantum Subroutines

To show case how $T_{GSA}$ can be combined with quantum phase estimation (QPE), in Fig. 9, we define define a quantum circuit with three registers. The first two registers carry information of the irreps and the quantum state of our many-body system while the last register with $n$ qubits is the ancilla used for QPE. We define the symmetry-adapted quantum phase estimation as $V_{\text{SQPE}} = U_{\text{QPE}} T_{\text{GSA}}$. This unitary performs a symmetry-controlled quantum phase estimation for a desired irrep, as follows

$$
\begin{aligned}
&V_{\text{SQPE}} |0\rangle^m |\psi\rangle |0\rangle^n \\
&= \sum_{u,v}^{2^n-1} \sum_{\Gamma} \frac{e^{-i2\pi v(E_\Gamma - u/2^n)}}{2^n \sqrt{d_\Gamma}} |\Gamma\rangle |\psi^\Gamma\rangle |u\rangle,
\end{aligned} \quad (23)
$$

for $d_\Gamma$ being the dimension of the irrep $\Gamma$. This circuit allows us to determine the energy $E_\Gamma$ when the system is restricted to a desired irrep $\Gamma$. After measuring the first and last registers, we automatically project our quantum state $|\psi\rangle$ to a given irrep, with the projection prob-
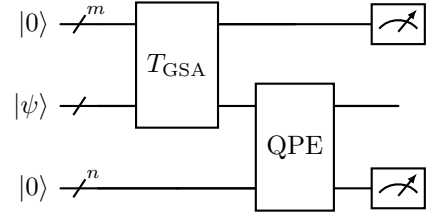


FIG. 9. Circuit for symmetry-adapted quantum phase estimation, where the first two registers carry information of the irreps and the quantum state $\psi$ of our many-body system, while the last register with $n$ qubits is the ancilla used for QPE. The input state $\psi$ is first decomposed into a coherent superposition of all irreps by $T_{\text{GSA}}$, and then a QPE or any other quantum subroutine can be applied to transform all irrep sectors of the quantum state simultaneously. The eigen energies and the irreps of quantum states will be stored in the first and the last register, where measurement (or amplitude amplification, not shown) can be performed to estimate the energies of states within a desired irrep.

ability to each irrep $\Gamma$ determined by the overlap between $|\psi\rangle$ and the state within an irrep $\Gamma$. This approach has many potential applications to diverse fields, ranging from quantum simulation to quantum chemistry. In the next sections we will use three examples to demonstrate how our approach works for abelian and non-abelian groups.

### B. One-dimensional Ising model in random transverse and longitudinal fields

In this section, we consider a simple example of a problem in condensed matter physics related to the irreps of the direct product group $G = \mathbb{Z}_N \times \mathbb{Z}_2$, where $\mathbb{Z}_N$ is a cyclic group of order $N = 2^n$.
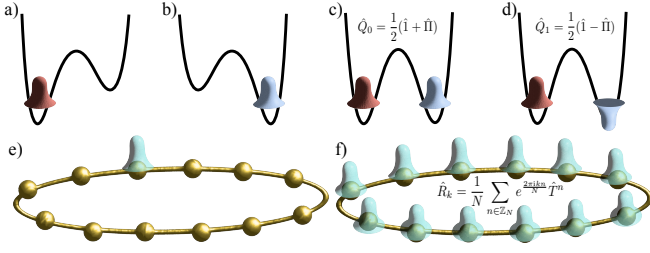
FIG. 10. Effect of the symmetry adapted transformation $T_{GSA}$ on the random Ising chain. a) Illustrate initial spin state breaking the parity symmetry of the Ising interaction term while b) depicts the effect of the parity operator on this initial state. c) and d) Illustrate the effect of the projectors $\hat{Q}_0$ and $\hat{Q}_1$. Similarly, e) shows a defect in the chain breaking translational symmetry. After applying the projector $\hat{R}_k$ into a desired momenta $k$, the state becomes translationally invariant as in f).

### 1. The one-dimensional quantum Ising model in random transversal and longitudinal fields

Consider the one-dimensional quantum Ising model in a random transverse and longitudinal fields [61, 62]

$$\hat{\mathcal{H}} = -\sum_{j=1}^{N} A_j X_j - J \sum_{j=1}^{N} Z_j Z_{j+1} - \sum_{j=1}^{N} K_j Z_j , \quad (24)$$

where $X_j, Y_j$ and $Z_j$ are Pauli matrices at the $i$-th site of the chain while $J$ denotes the coupling strength. The transverse $A_j \in [-W_T, W_T]$ and longitudinal $K_i \in [-W_L, W_L]$ fields are chosen from a random distribution of disorder with strengths $W_T$ and $W_T$, respectively. This model has a rich structure. For example, in the case of uniform transverse $A_j = A'$ and longitudinal $K_j = K'$ fields, this model is closely related to integrability breaking [63], level crossings [64], quantum many-body scars [65], and emergent exceptional group symmetry $E_8$ [66]. For the purposes of this section, we consider a chain with periodic boundary conditions $O_j = O_{j+N}$ with $O \in \{X, Y, Z\}$.

Next let us discuss the symmetries of Hamiltonian Eq. (24) in the absence of disorder ($W_T = W_L = 0$). In this case as the system has periodic boundary conditions and the interaction strength are uniform along the chain, the system is invariant under spatial translations $\hat{T}^\dagger O_j \hat{T} = O_{j+1}$ generated by the operator $\hat{T}$ and $[\hat{H}, \hat{T}] = 0$. Further, in the absence of the longitudinal field ($W_L = 0$), the model exhibits an Ising symmetry under the transformation $\hat{\Pi}^\dagger Z_j \hat{\Pi} = -Z_j$ with the parity operator $\hat{\Pi} = \bigotimes_{j=1}^{N} X_j$. In terms of groups, the translational invariance of the chain is related to the group $\mathbb{Z}_N$, while the Ising symmetry is related to $\mathbb{Z}_2$. If we consider these two symmetries, the combined symmetry group is given by $G = \mathbb{Z}_N \times \mathbb{Z}_2$. This symmetry group defines two good quantum numbers $k$ and $\sigma$, which are related

to momentum and parity, respectively.

### 2. Projection to symmetric subspaces without second quantization

Our goal in this section is to use the symmetry-adapted transformation to project a state with no symmetries to a desired symmetry subspace.

As we discuss in Appendix E, one can try to do a similar procedure by exploiting tools from condensed matter physics such as fermionization via the Jordan-Wigner transformation. All of these tools are available in second quantization and for the fermionic operators in real and momentum space. For example, one can identify the parity (Ising symmetry) subspaces by defining the right boundary conditions for the fermions and this also restricts the values of the momenta. In general, the second quantization approach does not simplify the problem and the treatment of the symmetries is obscure, as the Hamiltonian maps to a system of interacting fermions with highly nonlocal interactions.

In our approach, we will work directly with Pauli matrices in real space without using second quantization. It is important to consider a concrete example of a quantum state $|\psi\rangle = |110\ldots0\rangle$ with a localized domain wall that breaks both translational and Ising symmetries. To see this, one can act with the symmetry operations on this state obtaining $\hat{T}|\psi\rangle = |10\ldots01\rangle$ and $\hat{\Pi}|\psi\rangle = |001\ldots1\rangle$. Note that in the last expression, the string $001\ldots1$ is the bit-wise negation of $110\ldots0$ defining the state $|\psi\rangle$. After applying the symmetry-adapted transformation, we effectively obtain a state $|\psi^{k,\sigma}\rangle = \hat{P}^{k,\sigma}|\psi\rangle$, where $\hat{P}^{k,\sigma}$ is the projector defined in Eq. (22). This state is explicitly given by

$$|\psi^{k,\sigma}\rangle = \frac{1}{2N}(|110\ldots0\rangle + e^{-\frac{2\pi i k}{N}}|100,\ldots,1\rangle + \ldots) \quad (25)$$

$$+ \frac{(-1)^\sigma}{2N}(|001,\ldots,1\rangle + e^{-\frac{2\pi i k}{N}}|011\ldots0\rangle + \ldots$$

and has well defined momentum $k$ and parity $\sigma$. Other simple example is a state $|\psi\rangle = |000\ldots0\rangle$ with translational symmetry but breaking the Ising symmetry. After the projection we obtain a Greenberger–Horne–Zeilinger state (GHZ state) state.

$$|\psi^{0,\sigma}\rangle = \frac{1}{2}(|000\ldots0\rangle + (-1)^\sigma|111,\ldots,1\rangle) . \quad (26)$$

For this example, the only projector that survives is for the irrep labelled by $k = 0$. This state is very close to an exact energy eigenstate of the Ising chain with weak transverse field $g \ll J$ for a finite chain.

Next, let us explore the consequences of the symmetry adapted transformation when we calculate expectation values. Assume that we calculate the expectation value of the Hamiltonian Eq. (24) with disorder in the pro-

jected state $|\psi^{k,\sigma}\rangle = \hat{P}^{k,\sigma}|\psi\rangle$. We can explicitly write the expectation value $\langle\hat{\mathcal{H}}\rangle = \langle\psi|\hat{\mathcal{H}}_{k,\sigma}|\psi\rangle$

$$\hat{\mathcal{H}}_{k,\sigma} = [\hat{P}^{k,\sigma}]^\dagger \hat{\mathcal{H}} \hat{P}^{k,\sigma} = \hat{Q}_\sigma^\dagger \hat{R}_k^\dagger \hat{\mathcal{H}} \hat{R}_k \hat{Q}_\sigma \ , \qquad (27)$$

where $\hat{R}_k = 1/N \sum_{n\in\mathbb{Z}_N} e^{-\frac{2\pi i k n}{N}} \hat{T}^n$ and $\hat{Q}_\sigma = (\hat{1} + (-1)^\sigma \hat{\Pi})/2$ are projection operators into the symmetric subspaces labelled by $k$ and $\sigma$. Next, let us investigate the effect of the projection $\hat{Q}_\sigma$ on Hamiltonian

$$\hat{Q}_\sigma^\dagger \hat{\mathcal{H}} \hat{Q}_\sigma = \hat{Q}_\sigma \left( -\sum_{j=1}^N A_j X_j - J \sum_{j=1}^N Z_j Z_{j+1} \right) \ . \quad (28)$$

Comparing this with Eq. (24), we can see that as the longitudinal field $\sum_{j=1}^N K_j Z_j$ is odd under parity, the symmetry-adapted transformation removes this term.

After this, we can now calculate the projection into a given $k$ irrep. As the Ising interaction term is invariant under translations, the action of the projection on that term is trivial. The most interesting term is the random transverse field $\hat{\mathcal{H}}_T = -\sum_{j=1}^N A_j X_j$ because it explicitly breaks the translational invariance of the lattice and the projection acts in a nontrivial fashion on it, as follows

$$\hat{R}_k^\dagger \hat{\mathcal{H}}_T \hat{R}_k = \frac{1}{N^2} \sum_{n,m\in\mathbb{Z}_N} e^{-\frac{2\pi i k(n-m)}{N}} \hat{T}^{n-m} \left( -\sum_{j=1}^N A_{j+n} X_j \right)$$
$$= \frac{\hat{R}_k^\dagger}{N} \sum_{n\in\mathbb{Z}_M} e^{-\frac{2\pi i k n}{N}} \hat{T}^n \left( -\sum_{j=1}^N A_{j+n} X_j \right) \ . \quad (29)$$

After the projection, the Hamiltonian has translational invariance. The projection chooses an irrep with a well defined momentum $k$ that here acts as a label for the irreps of the translation group. The full projected Hamiltonian in Eq. (27) reads

$$\hat{\mathcal{H}}_{k,\sigma} = -\hat{R}_k^\dagger \hat{Q}_\sigma \sum_{n\in\mathbb{Z}_N} \frac{e^{-\frac{2\pi i k n}{N}} \hat{T}^n}{N} \sum_{j=1}^N A_{j+n} X_j$$
$$- J \hat{R}_k^\dagger \hat{Q}_\sigma \sum_{n\in\mathbb{Z}_N} \frac{e^{-\frac{2\pi i k n}{N}} \hat{T}^n}{N} \sum_{j=1}^N Z_i Z_{j+1} \ . \quad (30)$$

Here is important to note that the full Hamiltonian Eq. (24) couples all the irreps of the symmetry groups due to the disorder and the longitudinal field. What the projection is doing is to extract a diagonal block corresponding to irreps labeled by $k$ and $\sigma$.
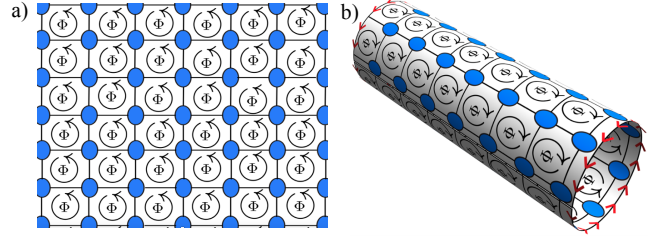


FIG. 11. The Harper-Hofstadter model. a) A two dimensional lattice of electrons under the effect of a magnetic field and b) the lattice with periodic boundary conditions defining the dynamics on a cylinder.

### C. Two-dimensional Harper-Hofstadter model

In the previous section we show how to use the symmetry adapted transformation to project a given quantum state into a desired combination of irreps of relevant symmetry groups of the system. In this section, we will go beyond this and show that one can effectively perform quantum phase estimation while restricting the system to a given irrep.

#### 1. The Harper Hofstadter model

After discussing the mathematical details of the group Fourier transform for $G = \mathbb{Z}_M$, also known as the quantum Fourier transform, it is instructive to investigate how our quantum circuit in Fig. 4 can be applied to a specific example. It is worth to remind the reader that in our work $\boldsymbol{x} = x_1 x_2 \cdots x_m$ denotes the binary representation of an integer defined by $x = x_1 2^{m-1} + x_2 2^{m-2} + x_m 2^0$.

We will apply our circuit for symmetry-adapted quantum phase estimation to resolve the energy spectrum of the Harper-Hofstadter model, a paradigmatic model of condensed matter physics [67]. In its original form, the Harper Hofstadter model describes a two dimensional system of electrons on a lattice under the effect of a magnetic field (see Fig. 11) governed by the Hamiltonian

$$\hat{\mathcal{H}} = J_x(\hat{\mathcal{U}}_b + \hat{\mathcal{U}}_b^\dagger) + J_y(\hat{\mathcal{V}}_b + \hat{\mathcal{V}}_b^\dagger) \ . \qquad (31)$$

This Hamiltonian is written a linear combination of two unitaries $\hat{\mathcal{U}}_b = \sum_{x,y} |\boldsymbol{x},\boldsymbol{y}\rangle \langle \boldsymbol{x+1},\boldsymbol{y}|$ and $\hat{\mathcal{V}}_b = \sum_{x,y} e^{2i\pi x b} |\boldsymbol{x},\boldsymbol{y}\rangle \langle \boldsymbol{x},\boldsymbol{y+1}|$ known as magnetic translations. The first term is responsible for the motion along the $x$ direction. The second term is responsible for the motion along the $y$ direction and it carries the effect of the magnetic field, as we depict in Fig. 11. In a quantum computer, the evolution under this Hamiltonian can be seen as a unitary $U = e^{-i\hat{\mathcal{H}}t}$ acting on two sets of registers $|\boldsymbol{x}\rangle$ and $|\boldsymbol{y}\rangle$ encoding the element $(x,y)$ the group $\mathbb{Z}_M \times \mathbb{Z}_M$. The integer shift $|\boldsymbol{x}\rangle \mapsto |\boldsymbol{x+1}\rangle$ can be implemented in a quantum computer by using the circuit

in Fig. (2).

The magnetic translations have very interesting algebraic properties. For example, if we calculate the action of the operators acting on different order

$$\hat{\mathcal{V}}_b \hat{\mathcal{U}}_b \left| \boldsymbol{x}, \boldsymbol{y} \right\rangle = e^{2i\pi(x-1)b} \left| \boldsymbol{x} - \boldsymbol{1}, \boldsymbol{y} - \boldsymbol{1} \right\rangle$$

$$\hat{\mathcal{U}}_b \hat{\mathcal{V}}_b \left| \boldsymbol{x}, \boldsymbol{y} \right\rangle = e^{2i\pi x b} \left| \boldsymbol{x} - \boldsymbol{1}, \boldsymbol{y} - \boldsymbol{1} \right\rangle \ , \qquad (32)$$

we obtain the relation $\hat{\mathcal{U}}_b \hat{\mathcal{V}}_b = e^{2i\pi b} \hat{\mathcal{V}}_b \hat{\mathcal{U}}_b$. For irrational $b$, this algebra is known as the quantum torus in non-commutative geometry [68].

The relation between the lattice constant of the lattice and the magnetic length leads to interesting effects [67]. For example, the spectrum is a fractal when it is plotted as a function of the magnetic field. Such a fractal spectrum is known in the literature as the Hofstadter butterfly [67] and it has been realized in quantum simulators [69]. Beyond condensed matter physics, the Harper-Hoftstadter model plays a very important role in the study of Mathieu operators [70], magnetic quantum walks [71] and non-commutative geometry in mathematics [68].

Due to the lattice symmetries and as we show in Appendix F, one we can show that Eq. (31) transforms under $U_{\mathrm{QFT}}$ for the vertical direction [labeled by $y$ in Eq. (32)] as $U_{\mathrm{QFT}} \hat{\mathcal{H}} U_{\mathrm{QFT}}^\dagger = \sum_k \hat{\mathcal{H}}_{k_y} \otimes \left| \boldsymbol{k_y} \right\rangle \left\langle \boldsymbol{k_y} \right|$ with $H_{k_y}$ defined as

$$\hat{\mathcal{H}}_{k_y} = \sum_x J_x e^{2i\pi(xb - k_y/N)} \left| \boldsymbol{x} \right\rangle \left\langle \boldsymbol{x} \right|$$

$$+ \sum_x J_y \left| \boldsymbol{x} \right\rangle \left\langle \boldsymbol{x} + \boldsymbol{1} \right| + \mathrm{H.c} \ . \qquad (33)$$

Let us consider the particular example $b = 1/2$ defining a rational magnetic translation. For this value, the magnetic translations anticommute $\hat{\mathcal{U}}_{1/2} \hat{\mathcal{V}}_{1/2} = -\hat{\mathcal{V}}_{1/2} \hat{\mathcal{U}}_{1/2}$. In terms of lattice symmetries, there is an effective dimmerization of the lattice in the horizontal axes. This is originated from the relation $\hat{\mathcal{U}}_{1/2} \hat{\mathcal{V}}_{1/2}^2 = \hat{\mathcal{V}}_{1/2}^2 \hat{\mathcal{U}}_{1/2} = \hat{\mathcal{U}}_{1/2}^2 \hat{\mathcal{V}}_{1/2} = \hat{\mathcal{V}}_{1/2} \hat{\mathcal{U}}_{1/2}^2$. That is, a magnetic translation by two lattice constants leaves the system invariant. In other words, by choosing $b = 1/2$ our system defines an effective pseudo-spin that tremendously simplifies the problem. The pseudospin structure emerges by considering even $x = 2n$ and odd $x = 2n - 1$ sites with integer $n$. The even sites are affected by an onsite potential $J_x^{\mathrm{Even}} = J_x e^{-2i\pi k_y/N}$, while the potential for odd sites is $J_x^{\mathrm{Odd}} = -J_x e^{-2i\pi k_y/N}$. Now, to fully describe the system we can define a ket $\left| \boldsymbol{n}, \Lambda \right\rangle$, where $n = 0, 1, \ldots M/2$ labels the space and $\Lambda = \uparrow, \downarrow$ the pseudospin degree of freedom representing even and odd sites. By using this notation, we can write the Hamiltonian Eq. (33) as spin-1/2 particle moving in a lattice under the effect of a mag-
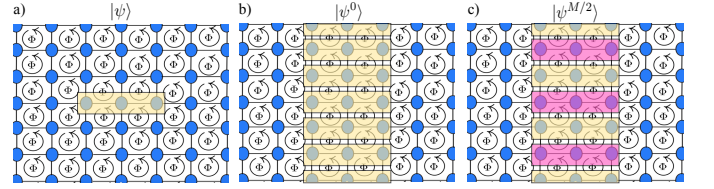


FIG. 12. Symmetry adapted projection of a quantum state. a) An initial state $\left| \psi \right\rangle = \sum_{x,y \in \mathbb{Z}_M} c_{x,y} \left| \boldsymbol{x}, \boldsymbol{y} \right\rangle$ that breaks the translational symmetry. Such a state is localized along three lattice sites. b) and c) The projections $\left| \psi^0 \right\rangle$ and $\left| \psi^{M/2} \right\rangle$ out of the state $\left| \psi \right\rangle$ as in a) into the irreps $k = 0$ and $k = M/2$, describing a long- and short-wavelength excitations in the lattice, respectively. We assume periodic boundary conditions along the $y$ directions in the lattice, which effectively allows us to represent the system as a lattice on a cylinder as in Fig. 11 b).

netic field and spin-orbit coupling, as follows

$$\hat{\mathcal{H}}_{k_y} = \sum_n \left( J_x^{\mathrm{Even}} \left| \boldsymbol{n}, \uparrow \right\rangle \left\langle \boldsymbol{n}, \uparrow \right| + J_x^{\mathrm{Odd}} \left| n, \downarrow \right\rangle \left\langle \boldsymbol{n}, \downarrow \right| + \mathrm{H.c} \right)$$

$$+ \sum_n \left( J_y \left| \boldsymbol{n}, \uparrow \right\rangle \left\langle n, \downarrow \right| + J_y \left| n, \downarrow \right\rangle \left\langle \boldsymbol{n} + \boldsymbol{1}, \uparrow \right| + \mathrm{H.c} \right) \ . \qquad (34)$$

In terms of symmetries, the value $b = 1/2$ defines the symmetry group $\tilde{G} = \mathbb{Z}_{M/2} \otimes \mathbb{Z}_M$ that is a subgroup of $G = \mathbb{Z}_M \otimes \mathbb{Z}_M$. This structure can be generalized for any rational number of the form $b = p/q$, where $p$ and $q$ are coprimes on such a way that the system has a symmetry group $\tilde{G} = \mathbb{Z}_{M/q} \otimes \mathbb{Z}_M$. When $b$ is irrational, the symmetry group is solely determined by $G = \mathbb{Z}_M$ as the system has translational invariance only in the $y$ axis.

Geometrically, the irrep labels $k_y$ label foliation of the cylinder by lines. As we depict in Fig. 11 b), this correspond to a family of decoupled lattices along a cylinder. The irreps $k_y$ denote the modes of stationary waves in the $y$ direction.

### 2. Symmetry-adapted quantum phase estimation for the Harper model

Next, let us investigate the action of the quantum circuit of Fig. 9 for a state $\left| \psi \right\rangle = \sum_{x,y \in \mathbb{Z}_M} c_{x,y} \left| \boldsymbol{x}, \boldsymbol{y} \right\rangle$ with no translational invariance at all as we depict in Fig. 12 a). The symmetry adapted transformation in this case has the form

$$T_{\mathrm{GSA}} = (U_{\mathrm{QFT}} \otimes \hat{1}) \cdot \mathrm{SELECT}[\tilde{\rho}_{\mathbb{Z}_m}] \cdot (U_{\mathrm{QFT}}^{-1} \otimes \hat{1}) \ , \quad (35)$$

with the controlled group action defined as $\mathrm{SELECT}[\tilde{\rho}_{\mathbb{Z}_m}] = \sum_u \left| \boldsymbol{u} \right\rangle \left\langle \boldsymbol{u} \right| \otimes \rho(u)$. Here $\tilde{\rho}(u) = \rho(u)$ is a one-dimensional representation of the group element $u \in \mathbb{Z}_M$ acting as a translation $\rho(u) \left| \boldsymbol{x}, \boldsymbol{y} \right\rangle = \left| \boldsymbol{x}, \boldsymbol{y} + \boldsymbol{u} \right\rangle$. The explicit action of the symmetry adapted transfor-

mation reads

$$T_{\text{GSA}} |\mathbf{0}\rangle |\psi\rangle = \sum_{k_y \in \mathbb{Z}_M} |\mathbf{k_y}\rangle |\psi^{k_y}\rangle \ , \qquad (36)$$

where $|\psi^{k_y}\rangle = \frac{1}{M} \sum_{x,y,v \in \mathbb{Z}_M} c_{x,y} e^{-2\pi i k_y v/M} |\mathbf{x}, \mathbf{y} + \mathbf{v}\rangle$. Note that the first register in Eq. (36) keeps the information of a given irrep labelled by $k_y$, while the group element $v \in \mathbb{Z}_M$ acts as a translation of the ket $|\mathbf{x}, \mathbf{y}\rangle \mapsto |\mathbf{x}, \mathbf{y} + \mathbf{v}\rangle$. If we stop the circuit here and measure the first register in a irrep labelled by $k_y'$, we effectively project our state into the symmetry adapted state $|\psi^{k_y'}\rangle$.

Let us discuss for a moment the physical interpretation of this projector. The integer $k_y$ labels the irreps but it also defines the wavelength of the excitations in the system. Such a wavelength is defined as $\lambda_y = M/k_y$. That is, irreps with $k_y = 0$ represent long-wavelenght excitations with $|\psi^0\rangle = \frac{1}{M} \sum_{x,y,v \in \mathbb{Z}_M} c_{x,y} |\mathbf{x}, \mathbf{y} + \mathbf{v}\rangle$ while $k_y = M/2$ are rapidly oscillating excitations represented by $|\psi^{M/2}\rangle = \frac{1}{M} \sum_{x,y,v \in \mathbb{Z}_N} (-1)^v c_{x,y} |\mathbf{x}, \mathbf{y} + \mathbf{v}\rangle$ in our system. These states are illustrated in Figures 12 b) and c). What the projector does is to select a given wavelength in our system for a desired $k_y$ so that such irrep is fixed for quantum phase estimation in our circuit

$$V_{\text{SQPE}} |\mathbf{0}\rangle^m |\psi\rangle |0\rangle^n$$
$$= \sum_{u,v} \sum_{k} \frac{e^{-i2\pi v(E_{k_y} - u/2^n)}}{2^n} |\mathbf{k_y}\rangle |\psi^{k_y}\rangle |\mathbf{u}\rangle , \qquad (37)$$

where $E_{k_y}$ are the eigenvalues of $\hat{\mathcal{H}}_{k_y}$ in Eq (33).

In this section we demonstrated the versatility of our approach by decomposing a system into different irreps labeled by the intex $k_y$ denoting the irreps of the group $\mathbb{Z}_M$. After this decomposition, we briefly show how to apply QPE, a quantum subroutine that can be used to efficiently access the energies of a manybody system using quantum computers. In the case of the Hamiltonian $\hat{\mathcal{H}}_{k_y}$ in Eq (33), QPE enables us to obtain the energies $E_{k_y}$. After plotting them as a function of the parameter $b$ in Eq (33), one obtains the Hofstadter butterfly, which has fractal properties and has been observed in quantum simulators [69].

### D. Three-dimensional *ab initio* electronic structure

It is instructive to consider an example of a chemistry problem where can explicitly carry both our the group Fourier transformation and symmetry-adapted transformation $T_{\text{GSA}}$. One of the advantages of our example is that we work with the symmetric group and show that it can be use to project a problem in first quantization to a fermionic sector of interest for quantum simulation of electronic structure in quantum chemistry.

### 1. The $H_2$ molecule in first quantization

In this section we consider an example that shows a practical application of the QCT for $G = S_2$ in Eq. (15) to a two-electron problem in electronic structure. The simplest example one can think of is the molecule $H_2$. For convenience, we describe this two-electron system in the formalism of first quantization under the Born-Openheimer approximation. In atomic units, the Hamiltonian for the $H_2$ molecule reads

$$\hat{\mathcal{H}} = \sum_m \left( -\frac{\nabla_m^2}{2} - \sum_{\beta=1}^{2} \frac{Z_\beta}{|\mathbf{r}_m - \mathbf{R}_\beta|} \right) + \frac{1}{|\mathbf{r}_1 - \mathbf{r}_2|}$$
$$= \hat{\mathcal{O}}^{(1)}(\mathbf{r}_1) + \hat{\mathcal{O}}^{(1)}(\mathbf{r}_2) + \hat{\mathcal{O}}^{(2)}(\mathbf{r}_1, \mathbf{r}_2) , \qquad (38)$$

where $Z_\beta$ is the atomic number of the nucleus $\beta = 1, 2$, and $|\mathbf{r}_m - \mathbf{R}_\beta|$ is the distance between the mth electron and the nuclei labeled by $\beta$, while $r_{1,2}$ is the distance between the two electrons. The Hamiltonians $\hat{\mathcal{O}}^{(1)}(\mathbf{r}_1)$ and $\hat{\mathcal{O}}^{(1)}(\mathbf{r}_2)$ are the core Hamiltonians for electrons 1 and 2, respectively. As we are dealing with a two-particle system, the natural choice to build up our Hilbert space is to choose a tensor product basis of the individual states of the particles. We remark here that so far, we have not imposed any restriction on the symmetry of the wave function as we are working on first quantization.

Next, let us consider a minimal basis with only two 1s spatial orbitals $|\phi_1\rangle$ and $|\phi_2\rangle$ localized around the two nuclei labelled by 1 and 2. Due to the spatial symmetry of the $H_2$ molecule, it is convenient to define *gerade* (even parity, bonding) and *ungerade* (odd parity, anti-bonding) molecular orbital as a linear combination of molecular orbitals

$$|\Phi_1\rangle = [2(1 + S_{1,2})]^{-1/2}(|\phi_1\rangle + |\phi_2\rangle)$$
$$|\Phi_2\rangle = [2(1 + S_{1,2})]^{-1/2}(|\phi_1\rangle - |\phi_2\rangle) , \qquad (39)$$

where $S_{1,2}$ is the overlap integral between the 1s orbitals. By using this basis set, any quantum state can be written as a linear combination

$$|\psi\rangle = \sum_{j_1,\alpha_1;j_2,\alpha_2} C_{j_1,\alpha_1,j_2,\alpha_2} |j_1, \alpha_1\rangle \otimes |j_2, \alpha_2\rangle . \qquad (40)$$

Here $|j_m\rangle$ denotes the spatial orbitals with $j_m \in \{\Phi_1, \Phi_2\}$ while $|\alpha_m\rangle$ represent the spin degree of freedom with $\alpha_m = 0, 1$. The two-particle wave function in Eq. (40) is a linear combination of $D = 16$ basis states and for this reason is natural to encode the state using $N = 4$ qubits. The odd qubits encode the orbital information and the even qubits encode the spin of the electrons.

### 2. Labeling the fermionic versus bosonic sector

After discussing the basic aspects of $H_2$, we need to calculate the action of the symmetry-adapted group transformation $T_{\text{GSA}}$ [see circuit in Fig. 5] on a quantum state $|0\rangle |\Psi\rangle$ where the first register encodes a trivial irrep of the group and $|\Psi\rangle$ is the state of the molecule in first quantization as in Eq.(40)

$$T_{\text{GSA}} |0\rangle |\psi\rangle = \sum_{\Gamma} |\Gamma\rangle \hat{P}^{\Gamma} |\psi\rangle$$
$$= |0\rangle \hat{P}^0 |\psi\rangle + |1\rangle \hat{P}^1 |\psi\rangle , \qquad (41)$$

where the projector above is given by $\hat{P}^{\Gamma} = \frac{d_{\Gamma}}{|G|} \sum_{g \in G} \chi_{\Gamma}(g)\rho(g)$. In our case, the group elements of $S_2$ are $\{e, (12)\}$ and the characters are shown in TABLE II. Thus, the projectors for different irreps are given explicitly by

$$\hat{P}^b = \frac{1}{2}\chi_b(e)\text{I} + \frac{1}{2}\chi_b[(12)]\text{SWAP}_{1,3}\text{SWAP}_{2,4}$$
$$= \frac{1}{2}\left[\text{I} + (-1)^b\text{SWAP}_{1,3}\text{SWAP}_{2,4}\right], \qquad (42)$$

where $\chi_b(g)$ is the characters for the group element $b$ under the irrep $b$, for $b = 0, 1$ used for a qubit encoding of the irreps $(2,0), (1,1)$ of $S_2$ as in the character TABLE II. Here the SWAP gate acting on odd qubits allows performing a permutation of the orbitals and the SWAP acting on even qubits allows permuting the spin degrees of freedom. Let us look more carefully at the action of the operators on our quantum state in Eq. (40)

$$\hat{P}^b |\psi\rangle = \sum_{j_1,\alpha_1;j_2,\alpha_2} C_{j_1,\alpha_1,j_2,\alpha_2}$$
$$\times \left(|j_1,\alpha_1;j_2,\alpha_2\rangle + (-1)^b |j_2,\alpha_2;j_1,\alpha_1\rangle\right), \quad (43)$$

which gives us exactly the bosonic and fermionic representation in terms of permanents and the slater determinants.

To illustrate how the projector acts on the spin degree of freedom it is useful to consider a simple example. Let us assume an initial state $|\psi'\rangle = |\Phi_1,\uparrow\rangle \otimes |\Phi_1,\downarrow\rangle$. Then the projection in the fermionic sector reads

$$\hat{P}^1 |\psi'\rangle = \frac{1}{2}(|\Phi_1,\uparrow\rangle \otimes |\Phi_1,\downarrow\rangle - |\Phi_1,\downarrow\rangle \otimes |\Phi_1,\uparrow\rangle)$$
$$= \frac{1}{2}|\Phi_1,\Phi_1\rangle \otimes (|\uparrow\downarrow\rangle - |\downarrow,\uparrow\rangle). \qquad (44)$$

This state describes a two-electron system in the singlet state with the two electrons occupying the same spatial orbital. States such as $|\psi'\rangle = |\Phi_1,\uparrow\rangle \otimes |\Phi_1,\uparrow\rangle$ are projected out of the fermionic sector due to Pauli exclusion principle. For pedagogical reasons, in the last line, we separated the spatial and spin degrees of freedom to explicitly show that the two-electron system is in a spin singlet state.

Similarly, the following will produce a superposition of triplet and singlet states. Starting from the state

$$|\psi''\rangle = (I \otimes ZH \otimes X \otimes H) |0\rangle^{\otimes 4}$$
$$= \frac{|\Phi_1,\uparrow\rangle - |\Phi_1,\downarrow\rangle}{\sqrt{2}} \otimes \frac{|\Phi_2,\uparrow\rangle + |\Phi_2,\downarrow\rangle}{\sqrt{2}} \qquad (45)$$

and projecting it into the fermionic sector we have

$$|\psi\rangle_{\text{fermionic}} \equiv \hat{P}^1 |\psi''\rangle$$
$$= \frac{1}{4}\left[|\Phi_1,\Phi_2\rangle - |\Phi_2,\Phi_1\rangle\right] \left[|\uparrow,\uparrow\rangle - |\downarrow,\downarrow\rangle\right]$$
$$+ \frac{1}{4}\left[|\Phi_1,\Phi_2\rangle + |\Phi_2,\Phi_1\rangle\right] \left[|\uparrow,\downarrow\rangle - |\downarrow,\uparrow\rangle\right],$$
$$\qquad (46)$$

where the first line is a triplet state, while the second line is a singlet state.

### 3. Labeling the singlet versus triplet sector

Figure 13 is a quantum circuit that achieves the symmetry-adapted transformation for the $H_2$ molecule discussed in previous section, composing a register representing the initial state in Eq. (45) plus the ancilla qubits for manipulating and labeling the irreps. For this initial state, the first part of the circuit allows one to label the bosonic and fermionic sectors, while the second part is the selection of the singlet and triplet sectors. A final measurement is performed on the two ancilla qubits if needed to post-select the desired irrep. Note that the post-selection success probability for a given irrep sector $\Gamma$ is given by $|a_\Gamma|^2$ as defined in Eq. (3).
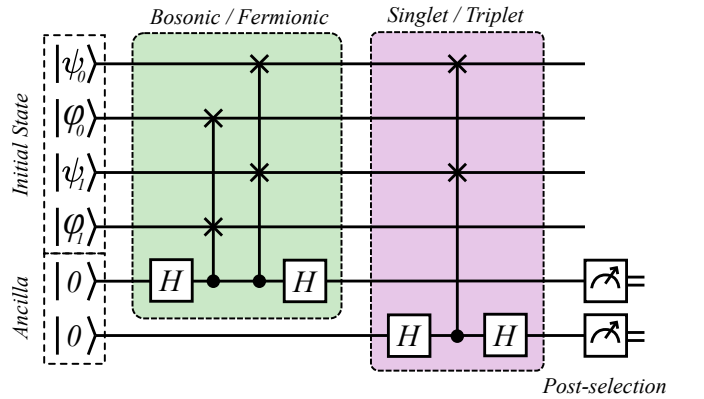


FIG. 13. Quantum circuit depicting the implementation of projectors $\hat{P}^b$ to project an initial state of the $H_2$ molecule to different irreps in 1st quantization encoding. Starting from initial state (first 4 qubits) with two ancilla qubits, the circuit in the green box labels the fermionic and bosonic sector using the first ancilla qubit. The circuit in the purple box then labels the singlet and triplet states using the last ancilla qubit.

Using standard quantum computing framework such as Qiskit [72], we can simulate the circuit in Fig. 13 and

obtain the resulting system density matrix after post-selecting the corresponding sectors. Fig. 14 shows the resulting density matrix of the system register from the exact and the noisy simulations. The noisy simulation was done using the fake provider module in Qiskit, which contains a fake (simulated) backend that mocks the IBM devices, *fake_7q_pulse_v1*. It can be seen that the singlet and triplet sectors, represented by the red and blue boxes in Fig. 14, respectively, have the same non-zero matrix values location within the complete density matrix representation.
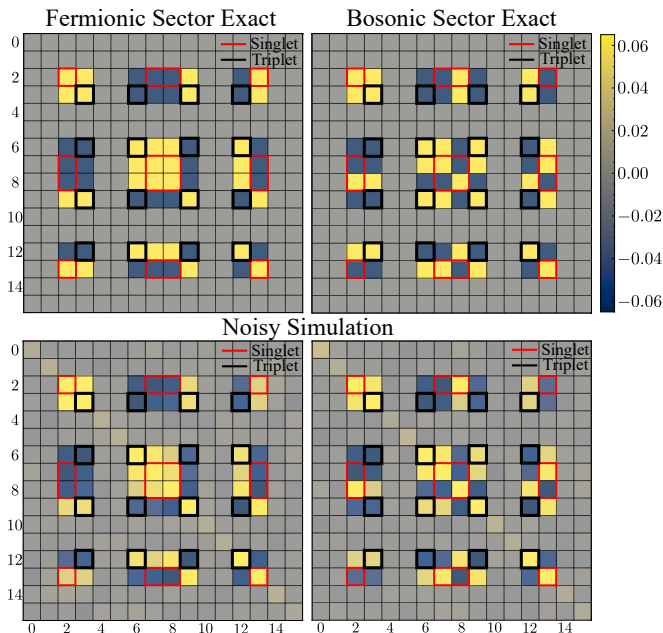


FIG. 14. Final density matrix of the $H_2$ molecule, post-selected on the two ancilla qubits (last two qubits in Fig. 13) that labels the fermionic vs. bosonic or singlet vs. triplet states.

Figure 15 presents a comparison of the diagonal elements of the density matrix shown in Fig. 14 for the $H_2$ molecule for different symmetry states. The comparison includes values from a noiseless simulation using the IBM local simulator, results from IBM Nazca (127-qubit) quantum computer, and the theoretical values. Here, in both cases we run the quantum circuit and obtain 10000 shots to get the output with reduced random error since the output is probabilistic in nature. The noiseless simulation agrees perfectly with the exact results, whereas the hardware results exhibit some deviations, which are attributed to the noise in the quantum hardware.

### 4. Symmetry-adapted quantum phase estimation for $H_2$

We can further combine the $T_{GSA}$ symmetry transform with quantum phase estimation as shown in Fig. 9 to estimate the energy of singlet and triplet state simultaneously. Fig. 16 shows the simulated energies correspond-
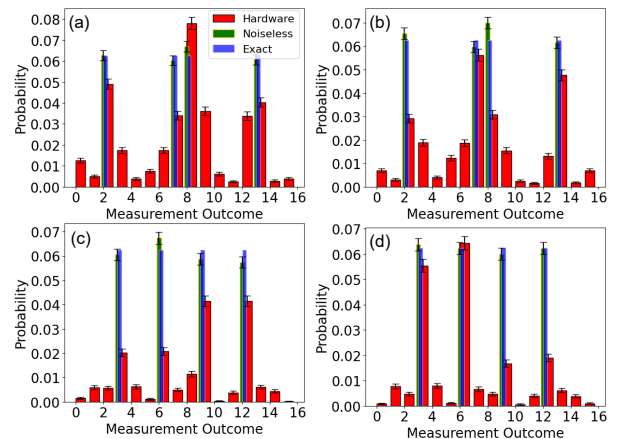


FIG. 15. Diagonal elements of the density matrix of the $H_2$ molecule, (a) singlet bosonic state, (b) singlet fermionic state, (c) triplet bosonic state and (d) triplet fermionic state.

ing to highest count state across different irreps versus the number of ancilla qubits in QPE. The symmetry-adapted QPE circuit was run with 2000 shots in IBM local simulator in a noiseless environment. The dashed red horizontal line in the plot shows the eigenvalues of the corresponding state obtained from the exact diagonalization of the Hamiltonian of the $H_2$ molecule. The results demonstrate that symmetry-adapted QPE can accurately predict the eigenenergies across different irreps. Note that besides the singlet and triplet states for $H_2$ in the case of fermionic particles, the other sectors represent fictitous state of the $H_2$ Hamiltonian with two bosonic particles that can be in singlet and triplet states. In this case, if the spin degree of freedom is in the singlet state, the spatial wave function should be antisymmetric to preserve the bosonic statistics of the particles.

## IV. OPEN PROBLEMS

The simulation of many-body quantum systems has been one of the most promising avenues toward quantum advantage since its original exposition by Feynman [73]. As discussed in this paper, an adequate treatment of symmetries in simulating interacting many-body systems on quantum computers opens new possibilities for additional quantum advantage. As the beginning of the endeavor for systematic treatment of symmetries of simulating many-body problems on quantum computers, our work inspires a plethora of important open problems that will be instrumental to quantify quantum advantage for quantum simulations.

We summarize some of the key questions in this section, including symmetries related to quantum chemistry in Sec. IV A and composite fermions and physical laws in Sec. IV B. Sec. IV C is devoted to open problems regarding quantum simulation on novel quantum comput-
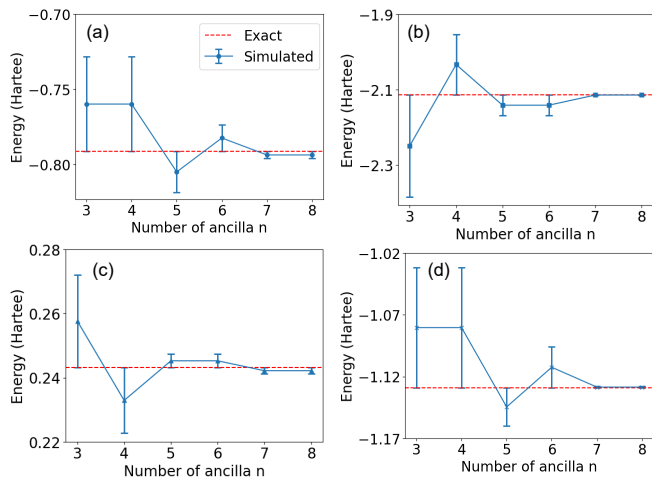
FIG. 16. Simulated energy by using our symmetry-adapted QPE algorithm for (a) singlet bosonic, (b) singlet fermionic, (c) triplet bosonic, and (d) triplet fermionic states of the $H_2$ molecule. The horizontal axis is the number of ancilla qubits $n$ in the 3rd register of Fig. 9. 2000 shots are used for the simulation.

ers that are composed of both continuous (e.g., bosonic modes) and discrete (e.g., qubits) variable components. Lastly, Sec. IV D provides remarks on practical quantum advantages of symmetries in quantum simulation.

### A. Quantum Chemistry

Physical systems often exhibit more symmetries beyond the cyclic shift and permutation group investigated above. For example, a full description of quantum chemistry (including rotation, vibration, and nuclei spins) requires a tensor product of the following five groups [74]: $E(3) \otimes SO(3) \otimes S_n^{(e)} \otimes G^{\mathrm{CNP}} \otimes \mathcal{E}$, where $E(3)$ is the three-dimensional Euclidean translation group, $SO(3)$ is the continuous rigid-body rotation of molecules, $S_n^{(e)}$ is the permutation of $n$ electrons, $G^{\mathrm{CNP}}$ is the complete nuclear permutation group for identical nuclei in a molecule, and $\mathcal{E}$ is the inversion of the coordinates of all particles (electrons, nuclei) in the center of mass of the molecule. To describe these symmetries, the following questions immediately arise:

• A general recipe to construct quantum circuits for the Quantum Character Transform (QCT) of general groups include non-Abelian and continuous groups is needed. The efficiency of such circuits often relies on recursive representation of the branching diagrams of groups [55]. Therefore, developing proper ways to encode the branching diagrams on quantum computers is an important sub-problem.

• A related mathematical question is that characters for many groups are unknown beyond the symmetric group and unitary group. The characters are important to construct efficient quantum circuits to realize the QCT.

• In addition to QCT, how to best realize generalized phase estimation on digital quantum computers to project into particular irreps of continuous groups is unclear. To achieve this, the construction of the projector in Eq. (A2) has to involve an integral over a continuous set of group elements (instead of the sum). On a digital quantum computer, proper discretization of the continuous group has to be developed, for example, by introducing $t$-design for the continuous group [75, 76].

• For quantum chemistry applications, an important scenario is that the continuous $SO(3)$ rotational symmetry can be broken into discrete point group symmetries [6] for highly symmetric molecules. Tackling these spatial symmetries will require local unitary operations on the spatial registers instead of spin registers in the 1st quantization mapping. The design of these local operations will depend on basis set [77] choice in quantum chemistry and careful quantification of the circuit complexity needs further analysis.

• Another major class of molecules in quantum chemistry are transition-metal complexes with spin-orbital coupling [78, 79]. To investigate this, one need to implement local unitary operations that mix spin and spatial registers. Moreover, important applications such as calculating the natural lifetime of electronic states will require a relativistic treatment based on the Dirac equation or its reduced version [80, 81]. A full four-component wave function (including positron) in the 1st-quantization may be required to fully leverage symmetries in quantum simulation of these relativistic systems.

Note that most of these questions also apply to material science simulation in general, with slight changes of basis sets and the underlying symmetries.

### B. Composite Fermions and Physical Laws

Beyond quantum chemistry problems, simulating quantum systems with composite or continuous-variable degrees of freedom (for example bosonic modes) has become increasingly important [82, 83]. These inspires the following questions:

• Mathematically, fermions and bosons are associated to irreps of the permutation group acting on $N$ particles in (3+1)-dimensions (three spatial dimensions plus time). However, certain low-dimensional strongly interacting electronic systems can host emergent quasiparticles with exotic statistics such as in the fractional quantum Hall effect in (2+1) dimensions [84]. There, electrons and flux quanta form states known composite fermions [85]. The symmetry group associated to fractional quantum Hall states is the braid group and the quasiparticles above the ground state are referred to as anyons [86]. It remains a challenge to simulate these fermionic systems using quantum computers and our approach could be useful to perform this simulation in first quantization.

• Beyond simple Dirac fermions emerging in effective theories for graphene [87] and the quantum Ising model [88], SU($N$) fermions [89] are an important class of particles in condensed matter systems exhibiting non-abelian symmetries [90, 91]. These systems can be experimentally realized in available quantum simulators [92, 93]. However, further investigation is required to better leverage symmetry quantum subroutines to treat such SU($N$) fermions. This is of utmost importance in condensed matter systems to explore exotic states of matter such as heavy fermions [94] and spin liquids [95].

• Fundamental interactions have their own symmetries that are intimately related to the physical laws. For example, the grand unification theory suggests $SU(3) \times SU(2) \times U(1)$ symmetries are sufficient to capture the three fundamental interactions [2]. How to encode these symmetries of physical laws (instead of symmetries of individual quantum systems) into quantum simulation deserves more study.

• By discretizing the quantum fields, lattice gauge theory requires the quantum simulation of boson-fermi-spin mixed systems [83]. Mapping them to quantum computers and leveraging symmetry subroutines to speedup the simulation are important problems to investigate.

### C. Symmetries on Hybrid Quantum Computers

On the flip side, what if the quantum computers themselves are governed by different symmetries? For example, significant progress has been made on hybrid oscillator-qubit quantum processors [96]. Given such a hybrid continuous-variable (CV) and discrete-variable (DV) quantum computer, how symmetry transformation should be constructed and encoded in a different fashion as compared to qubit-based quantum computers? Can the CV degrees of freedom on the quantum computer help us better perform group Fourier transform for continuous groups?

One important use of hybrid CV-DV quantum processor is to encode logical qubits into the CV bosonic modes to realize bosonic quantum error-correction [97, 98]. Preparation of bosonic code words can be viewed as a projection from an initial CV vacuum state to rotational-symmetric (e.g., cat code) [99] or translational-symmetric (e.g., GKP code) [100] CV state. One natural question is whether it is possible to use symmetry transformation to prepare such code word? If so, how to construct these symmetry transformations using native universal gate sets on hybrid CV-DV quantum computers? Moreover, would this way of formulating bosonic code preparation inspire new bosonic codes to be designed based on a wider class of symmetry groups?

### D. Remarks on Quantum Advantage

Above all the technical development, the most important question is to identify where exponential speedup could come from in quantum simulations [101–106], given proper treatment of symmetries on quantum computers. Obviously, it is important to quantify the gate complexity of the symmetry-adapted quantum simulation routine itself. We emphasize here a few additional considerations:

• One important aspect is the state preparation problem for quantum simulation [102, 107–109]. Namely, a simple initial product state is usually transformed to a linear combination of symmetry-adapted final states (Eqs. (45) and (46)). It is not clear how to best design the preparation of the initial product state given a desired target final state. For example, how does the use of non-Clifford gates in the product state preparation affect the coverage or weight of the final state over all irreps of the group. The approach presented in the current work may shed new light on the state preparation problem [102].

• The answer to quantum advantage also strongly depends on what observables are measured after the quantum simulation, because extraction of any classical information from quantum computers has to pay a non-negligible cost [110–112]. In the presence of symmetry transformations, we conjecture that measuring properties related to symmetries of the physical system may better leverage the advantage brought by symmetry-adapted quantum simulation.

• For *ab initio* quantum simulation, an important aspect (despite often ignored) is how to design or pick the best basis set to discretize the original continuous problem [77, 113–115]. Standard basis in quantum chemistry are often used for simulation on quantum computers. However, it is not clear that existing basis sets that work the best on classical computers will necessarily be the choice for quantum computers.

• In NISQ era, quantum computers often suffer from noise and decoherence. However, the symmetry of noise may be entirely different than the symmetry of the many-body quantum system under investigation. For example, coherent noise can be viewed as a special symmetry, which has been leveraged to construct novel algorithmic-level error-correction strategy [116]. This suggests that symmetry transformation in the current work might provide a way to design quantum simulation algorithms that are less sensitive to noises, where Ref. [42, 43] provide excellent examples on such endeavor.

The challenge of quantifying practical quantum advantage lies in carefully integrating all the above aspects at each individual layer to derive concrete end-to-end resource estimation with a clearly defined resource metric.

## V. CONCLUSIONS AND OUTLOOK

In summary, we formulated a unified framework for treating symmetries in quantum simulation of many-body physics given quantum computers. We provided concrete circuit constructions and resource estimations for symmetry-adapted projection for common groups and pairs of groups in many-body physics. We further demonstrate the power of these symmetry-adapted routines, i.e., the generalized phase estimation, by combining them with other quantum simulation subroutines such as quantum phase estimation. Example applications to important condensed matter and quantum chemistry problems ranging from 1D to 3D are discussed. The provable speedups of these symmetry-adapted quantum subroutines suggests their applicability in fault-tolerant era. The symmetry-adapted quantum phase estimation circuit for a small molecule under minimal basis is also executed on noisy quantum hardware, demonstrating the practicality of our framework for NISQ era as well. We conclude the paper with a thorough discussion of major open problems regarding symmetries in simulation of many-body systems on quantum computers. We hope the unified framework and the related open problems presented in this work serve as a solid stepping stone for future endeavors exploring practical and provable quantum advantages of simulation of many-body quantum systems in the NISQ and fault-tolerant era.

## Appendix A: Character derivation of $T_{\text{GSA}}$

The $T_{\text{GSA}}$ can be thought of as a linear combination of projection operators associated to the irreps. The projector $\hat{P}^\Gamma$ into the irrep $\Gamma$ can be derived directly from the characters only. Hence, this allows an easier construction for groups with irreps of dimension larger than one.

To derive the projection operator equations into an irreducible representation (irrep) using characters, we will utilize the orthogonality relations of characters and the properties of irreducible representations. This approach leverages the fact that characters are invariant under conjugation and provides a simpler way to project onto irreducible subspaces.

The character $\chi_\Gamma(g)$ of an element $g$ in the $\Gamma$-th irrep is the trace $\chi_\Gamma(g) = \sum_i D^\Gamma_{ii}(g)$ of the representation matrix $\boldsymbol{D}^\Gamma(g)$. The orthogonality relation for characters is given by

$$\frac{1}{|G|}\sum_{g\in G}\chi_\Gamma(g)\chi_{\Gamma'}(g^{-1}) = \delta_{\Gamma,\Gamma'}\;, \quad (A1)$$

where $|G|$ is the order of the group, and $\delta_{\Gamma,\Gamma'}$ is the Kronecker delta. Using this relation, the projection operator $\hat{P}^\Gamma$ into the $\Gamma$-th irrep can be derived using the characters of the group elements. The goal is to construct an operator that projects any quantum state $|\psi\rangle$ into the subspace, transforming according to the $\Gamma$-th irrep. The projection operator $\hat{P}^\Gamma$ for the $\Gamma$-th irrep can be defined as:

$$\hat{P}^\Gamma = \frac{d_\Gamma}{|G|}\sum_{g\in G}\chi^*_\Gamma(g)\rho(g)\;, \quad (A2)$$

where $d_\Gamma$ is the dimension of the $\Gamma$-th irrep and $\chi_\Gamma(g)$ is the character of $g$ in the $\Gamma$-th irrep. $\rho(g)$ is the unitary representation of the group element $g$. To see how this works, the action of the projection operator on $|\psi\rangle$ is:

$$\hat{P}^\Gamma|\psi\rangle = \frac{d_\Gamma}{|G|}\sum_{g\in G}\chi^*_\Gamma(g)\rho(g)|\psi\rangle\;. \quad (A3)$$

Here, $\rho(g)$ acts on the Hilbert space of $|\psi\rangle$.

Next we prove that Eq. (A2) is a projector. To do this, we need to check that applying $\hat{P}^\Gamma$ twice yields the same result as applying it once:

$$\hat{P}^\Gamma\hat{P}^\Gamma = \hat{P}^\Gamma\;. \quad (A4)$$

To show this, let us start by substituting Eq. (A3) into (A4)

$$\hat{P}^\Gamma\hat{P}^\Gamma = \left(\frac{d_\Gamma}{|G|}\sum_{g\in G}\chi^*_\Gamma(g)\rho(g)\right)\cdot\left(\frac{d_\Gamma}{|G|}\sum_{g'\in G}\chi^*_\Gamma(g')\rho(g')\right)$$
$$= \frac{d_\Gamma^2}{|G|^2}\sum_{g\in G}\sum_{g'\in G}\chi^*_\Gamma(g)\chi^*_\Gamma(g')\rho(g)\rho(g')\;. \quad (A5)$$

Next, we can use the definition of homomorphism $\rho(g)\rho(g') = \rho(gg')$ to obtain the relation

$$\hat{P}^\Gamma\hat{P}^\Gamma = \frac{d_\Gamma^2}{|G|^2}\sum_{g\in G}\sum_{g'\in G}\chi^*_\Gamma(g)\chi^*_\Gamma(g')\rho(gg')\;. \quad (A6)$$

The next step is to define a new variable $j = gg'$ such that $g = jg'^{-1}$. After reindexing, we obtain

$$\hat{P}^\Gamma\hat{P}^\Gamma = \frac{d_\Gamma^2}{|G|^2}\sum_{j\in G}\sum_{g'\in G}\chi^*_\Gamma(jg'^{-1})\chi^*_\Gamma(g')\rho(j)\;. \quad (A7)$$

After using the homomorphism $\chi_\Gamma^*(jg'^{-1}) = \chi_\Gamma^*(j)\chi_\Gamma^*(g'^{-1})$ and the orthogonality relation in Eq. (A1) we obtain

$$
\begin{aligned}
\hat{P}^\Gamma \hat{P}^\Gamma &= \frac{d_\Gamma^2}{|G|^2} \sum_{j\in G}\sum_{g'\in G} \chi_\Gamma^*(j)\chi_\Gamma^*(g'^{-1})\chi_\Gamma^*(g')\rho(j) \\
&= \frac{d_\Gamma}{|G|} \sum_{j\in G} \chi_\Gamma^*(j)\rho(j) \qquad\qquad \text{(A8)}\\
&= \hat{P}^\Gamma \ .
\end{aligned}
$$

Thus, $\hat{P}^\Gamma$ is indeed a projection operator. In the case of abelian groups, all the irreps are one-dimensional and this can be applied in the same fashion as the $T_{\text{GSA}}$ by summing over all irreps

$$
\begin{aligned}
T_{GSA}|0\rangle \otimes |\psi\rangle &= \sum_\Gamma \frac{d_\Gamma}{|G|}\sum_{g\in G}\chi_\Gamma(g)|\Gamma\rangle \otimes \rho(g)|\psi\rangle \\
&= \sum_\Gamma a_\Gamma |\Gamma\rangle \otimes |\psi^\Gamma\rangle , 
\end{aligned}
\tag{A9}
$$

giving the projection of $|\psi\rangle$ into the irrep subspaces $\psi^\Gamma$ weighted by $a_\Gamma$.

### Appendix B: Projection Circuits

If we are just interested in projecting into a given irrep $\Gamma$, we can implement the projection equations exactly at the cost of a uniform normalization factor

$$
\begin{aligned}
\frac{1}{\mathcal{N}}\sum_\Gamma \hat{P}^\Gamma |\psi\rangle &= \frac{1}{\mathcal{N}}\sum_\Gamma \frac{d_\Gamma}{|G|}\sum_C \chi_\Gamma^*(C)\cdot\sum_{g\in C}^{|C|}\rho(g)|\psi\rangle \\
&= \frac{1}{\mathcal{N}}\sum_\Gamma a_\Gamma |\psi^\Gamma\rangle .
\end{aligned}
\tag{B1}
$$

The normalization constant is given by $\mathcal{N} = \sqrt{\sum_\Gamma \frac{d_\Gamma^2}{|G|}}$. In this case, a simplified circuit using just a PREPARE oracle can be used. The PREPARE is a state preparation oracle that stores the normalized coefficients in the first column of a unitary by acting on the $|0\cdots0\rangle$ ancilla state

$$
\text{PREPARE} = \frac{1}{\mathcal{N}}\sum_C^{N_{\text{Conj}}}\frac{d_C}{\sqrt{|G|}}|C\rangle\langle0|+\Pi_\perp = \begin{bmatrix} \frac{d_1}{\sqrt{|G|}} & \cdot & \cdots \\ \frac{d_2}{\sqrt{|G|}} & \cdot & \cdots \\ \vdots & \ddots & \cdots \\ \frac{d_{N_{\text{Conj}}}}{\sqrt{|G|}} & \cdot & \cdots \end{bmatrix}.
\tag{B2}
$$

where $\Pi_\perp$ is a projector to the orthogonal space in the rest of the matrix except the 1st column. The weighting coefficient is given by $d_\Gamma = d_C$. The rows of PREP

are group conjugacy classes $C$. The abstract circuit to implement the projector is shown in Fig. 17.
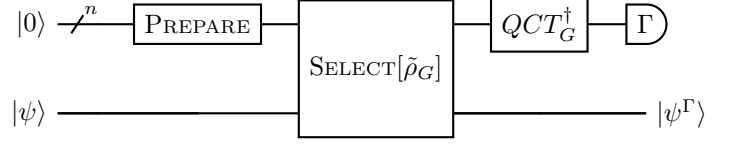


FIG. 17. Quantum circuit for $T_{GSA}$ showing projection of $|\psi\rangle$ onto irrep $\Gamma$ through post selection, where QCT is the quantum character transform as defined in Eq. (7).

The projection circuits for the cyclic group $\mathbb{Z}_M$ can be simplified with PREPARE($\frac{1}{\sqrt{2^n}}$), since we act on $n$- qubits where the state $\sum_C \frac{1}{\sqrt{2^n}}|C\rangle$ can be prepared by $H^{\otimes n}$ acting on the $|0\cdots0\rangle$ state. The overall circuit that is shown in Fig. 18, which takes a very similar form as the quantum phase estimation algorithm. However, we are not reading out on the ancilla qubits but explicitly projecting via post-selection for a given irrep $\Gamma$.

### Appendix C: Frobenius Character Formula

The characters of the symmetric group $S_N$ can be calculated by the Frobenius Character formula [49], simply from the coefficients of a multivariate polynomial of $x = x_1, x_2, \ldots, x_k$, where $k$ is the number of parts of a partition representing an irrep $\Gamma$

$$
\chi_\Gamma(C_\mu) = \left[\Delta(x)\cdot\prod_q P_q(x)^{j_q}\right]_{(l_1,\ldots,l_k)}, \tag{C1}
$$

where $\chi_\Gamma(C_\mu)$ is the character of a conjugacy class $C_\mu$ represented by the cycle type given by the partition $\mu = (m^{j_m},\cdots,2^{j_2},1^{j_1})$, where $j_q$ is the number of cycles of length $q$ in the cycle type of the conjugacy class $\mu$. $[\cdots]_{(l_1,\ldots,l_k)}$ means the coefficient of the monomial
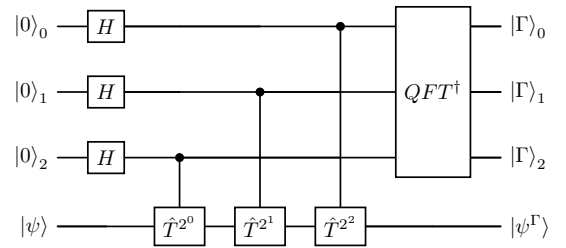


FIG. 18. Symmetry group transform for the cyclic group $\mathbb{Z}_8$, using an explicit projection circuit. Since the input state on the ancilla is the trivial irrep $|0\rangle_0 |0\rangle_1 |0\rangle_2$, the QFT in Fig. 4 can be simply replaced by a Hadamard transform in the above.

$x_1^{l_1} x_2^{l_2} \cdots x_k^{l_k}$ in Eq. (C1). $\Gamma$ is the irreducible representation corresponding to a partition $\Gamma = (\lambda_1, \lambda_2, ..., \lambda_k)$ of $k$ parts. We introduce an index shift $l_n = \lambda_n + k - n$ for each part $(l_1, \ldots, l_k)$. $\Delta(x)$ is the Vandermonde determinant defined as

$$\Delta(x) = \prod_{1 \le a < b \le k} (x_a - x_b) . \qquad (C2)$$

This determinant captures the antisymmetric properties of the conjugacy class, where $\Delta(\ldots, x_a, \ldots, x_b, \ldots) = -\Delta(\ldots, x_b, \ldots, x_a, \ldots)$, with each variable relating to a part of the partition $\lambda$. $P_q(x)$ is the power sum symmetric polynomial defined as

$$P_q(x) = x_1^q + x_2^q + \cdots + x_k^q . \qquad (C3)$$

This polynomial is used to encode each part of the cycle structure of the conjugacy class $C_\mu$. $\prod_q P_q(x)^{j_q}$ is the product of power sum polynomials raised to the powers corresponding to the cycle structure of the conjugacy class. Therefore, the coefficients of the polynomial encode the characters for a given cycle type $\mu$ for the various irreps related to the index $(l_1, \ldots, l_k)$. Other computational methods exist for calculating the characters of the symmetric group, such as those by Coleman [117].

## Appendix D: Group Fourier Transform

Let us start by defining the Fourier transform over a finite group $G$. In physics, we are all familiar with the notion of a Fourier transform. It allows us to map functions of time or time series to unveil their frequency spectrum. Similarly, in quantum information, one can define Fourier transforms associated to finite groups [118].

Now, consider a finite group $G$ of order $|G|$ and a quantum state $|\phi\rangle = \sum_g w_g |g\rangle$, where $|g\rangle$ is a convenient encoding of the group elements $g \in G$ into ancilla registers. The group Fourier transformation $F_G$ is a map from an arbitrary quantum state of the group elements $|\phi\rangle = \sum_g w_g |g\rangle$ to a new basis $\{|\Gamma, ij\rangle\}$, such that

$$F_G |\phi\rangle = \sum_g w_g F_G |g\rangle = \sum_{i,j} \sum_\Gamma W_{i,j}^\Gamma |\Gamma, ij\rangle . \qquad (D1)$$

Here $W_{i,j}^\Gamma$ are coefficients associated to irreducible representation $\Gamma$. The corresponding matrix is given explicitly by $\boldsymbol{W}^\Gamma = \sqrt{\frac{d_\Gamma}{|G|}} \sum_g w_g \boldsymbol{D}^\Gamma(g)$, where $\boldsymbol{D}^\Gamma(g)$ is the matrix representation of the irrep labeled by $\Gamma$ with matrix elements $D_{ij}^\Gamma(g)$. By taking the trace of this equation, we obtain a relation $\mathrm{tr}(\boldsymbol{W}^\Gamma) = \sqrt{\frac{d_\Gamma}{|G|}} \sum_g w_g \chi_\Gamma(g)$ to the characters $\chi_\Gamma(g) = \mathrm{tr}[\boldsymbol{D}^\Gamma(g)] = \sum_i D_{ii}^\Gamma(g)$ associated to the group element $g$ for the irrep $\Gamma$. The parameters $d_\Gamma$ denote the dimensions of the irrep $\Gamma$ and are related to the order of the group via $\sum_\Gamma d_\Gamma^2 = |G|$. In terms of the coefficients $w_g$ and $A_{i,j}^\Gamma$ the inverse transform can be

represented as

$$
\begin{aligned}
w_g &= \sum_\Gamma \sqrt{\frac{d_\Gamma}{|G|}} \mathrm{tr}[\boldsymbol{D}^\Gamma(g^{-1}) \boldsymbol{W}^\Gamma] \\
&= \sum_\Gamma \sum_{ij} \sqrt{\frac{d_\Gamma}{|G|}} D_{ji}^\Gamma(g^{-1}) W_{ij}^\Gamma(g) .
\end{aligned} \qquad (D2)
$$

The group Fourier transformation is unitary and it can be efficiently performed on a quantum computer [118], where a subgroup chain known as a Bratelli diagram is exploited. The group Fourier transform is explicit given by

$$F_G = \sum_\Gamma \sum_{ij} \sum_{g \in G} \sqrt{\frac{d_\Gamma}{|G|}} D_{ij}^\Gamma(g) |\Gamma, ij\rangle \langle g| , \qquad (D3)$$

where $\Gamma$ labels the irreps. The inverse Fourier transform is given by

$$F_G^{-1} = \sum_\Gamma \sum_{ij} \sum_{g \in G} \sqrt{\frac{d_\Gamma}{|G|}} [D_{ij}^\Gamma(g)]^* |g\rangle \langle \Gamma, ij| . \qquad (D4)$$

Within a irrep $\Gamma$, a group element $g$ is represented by a $d_\Gamma \times d_\Gamma$ matrix with elements $D_{ij}^\Gamma(g)$. The Quantum Character Transform can be obtained by tracing over the $i, j$ indices and factorizing on the conjugacy classes, which is a more compact way of representing the group Fourier transform for high-dimensional irreps.

### 1. Group Fourier transformation for the permutation group $S_n$

Let us briefly summarize the most important aspects of the group Fourier transform for the symmetric group $G = S_n$ for $n$ objects [55]. This group is finite with an order of $|G| = n!$ and its elements are permutations of $n$ objects. Given a permutation $g \in S_n$, one can decompose it as a product of elementary transpositions $c_{k,k+1}$. The irreps are then fully characterized in terms of partitions and Young diagrams. In fact, to build the representation $\Gamma_j$, we first need to calculate the representation of the elementary transpositions $c_{k,k+1}$ by looking at the weighted number of steps to reach two numbers in a given standard Young tableaux. For example, for $n = 2$, the order is $|S_2| = 2$ and there are two irreps $\Gamma_1 = (2,0) = \square\square$ and $\Gamma_2 = (1,1) = \begin{smallmatrix}\square\\\square\end{smallmatrix}$ that are one-dimensional. For $n = 3$ the order of the group is $|S_3| = 6$ and there are three irreps. $\Gamma_1 = (3,0) = \square\square\square$ and $\Gamma_2 = (2,1) = \begin{smallmatrix}\square\square\\\square\end{smallmatrix}$ and $\Gamma_3 = (1,1,1) = \begin{smallmatrix}\square\\\square\\\square\end{smallmatrix}$. The irreps $\Gamma_1$ and $\Gamma_3$ are one-dimensional, while $\Gamma_2$ is two-dimensional. The irrep $\Gamma_2$ is two-dimensional because there are two standard Young tableux $T_{A_1}^{\Gamma_2} = \begin{smallmatrix}1&2\\3\end{smallmatrix}$ and $T_{A_2}^{\Gamma_2} = \begin{smallmatrix}1&3\\2\end{smallmatrix}$ that act as basis

defining the matrix representation $D_{i,j}^{\Gamma_2}(g)$.

To define the group Fourier transform in Eq. (D3) for the symmetric group $G = S_n$ [29], we need to encode the irreps and the group elements using ancilla quantum registers. In order to do this, we use *canonical coding* of an element $g \in S_n$. This gives a concrete indexing scheme for elements with the implicit map back to permutations as follows:

$$(i_1, i_2, \cdots, i_{n-1}) \in \mathbb{Z}_2 \times \mathbb{Z}_3 \times \cdots \times \mathbb{Z}_n, \tag{D5}$$

$$g = c_{(1,2,\cdots,n)}^{i_{n-1}} \cdots c_{(1,2,3)}^{i_2} c_{(1,2)}^{i_1}. \tag{D6}$$

An indexing scheme can be generated from group elements following this decomposition as follows:

$$S_n \rightarrow \{g_i\}, \text{ with } i \equiv \sum_{j=1}^{n-1} i_j \frac{n!}{(j+1)!}, \tag{D7}$$

where this index is generated given any $g$ with the form of Eq. (D6) [55]. In general, for non-abelian groups, we also need to encode the label $\Gamma$ and the matrix indices $i, j$ and finally the group elements $g$ associated to the matrix representation $D_{i,j}^{\Gamma}(g)$. We refer the readers to Ref. [55] for further details on this encoding. Ref. [55] also provides an explicit construction of an efficient quantum circuit implementing the group Fourier transform for the symmetric group based on the group tower structure $S_1 \subset S_2 \cdots S_{n-1} \subset S_n$ with poly($n$) scaling.

Next, let us explicitly construct the group Fourier transform in Eq. (D3) for the permutation group of two particles $G = S_2$ with group elements $g \in S_2 = \{id, c_{(1,2)}\}$. Any group element can be encoded using a single qubit $|i_1\rangle$ as $g = c_{(1,2)}^{i_1}$ where $i_1 \in \mathbb{Z}_2$ as in the canonical encoding. More specifically, the canonical encoding of the group elements is given by $|id\rangle = |0\rangle$ and $|c_{(1,2)}\rangle = |1\rangle$.

As for $n = 2$, the irreps are one-dimensional, we do not need to encode the labels $i, j$ in the group Fourier transform of Eq. (D3). We can encode the irreps label using a single qubit, i.e., $|\Gamma_1\rangle = |0\rangle$ and $|\Gamma_2\rangle = |1\rangle$. By using these encodings, we obtain the explicit form for the group Fourier transform for $G = S_2$

$$
\begin{aligned}
F_{S_2} &= \sum_\Gamma \sum_{g \in S_2} \sqrt{\frac{d_\Gamma}{|S_2|}} D^\Gamma(g) |\Gamma\rangle \langle g| \\
&= \frac{1}{\sqrt{2}} (|0\rangle \langle 0| + |0\rangle \langle 1| + |1\rangle \langle 0| - |1\rangle \langle 1|) \\
&= \frac{1}{\sqrt{2}} \begin{bmatrix} 1 & 1 \\ 1 & -1 \end{bmatrix},
\end{aligned}
\tag{D8}
$$

where $d_\Gamma = 1$ and $|S_2| = 2$. Note that $D^{\Gamma_1}(id) = D^{\Gamma_2}(id) = D^{\Gamma_1}[c_{(1,2)}] = 1$ and that $D^{\Gamma_2}[c_{(1,2)}] = -1$. Thus, in the canonical representation, the group Fourier transform corresponds to a Hadamard gate $F_{S_2} = H$.

## Appendix E: Jordan-Wigner transformation and symmetries of interacting fermionic models

In the main text, we discussed a non-integrable spin model in Eq. (24). In this section, we will discuss symmetries of this model using standard tools of condensed matter physics to show its complexity. We will show that this model can be mapped to a system of interacting fermions in momentum space, albeit being highly non-local.

Pauli matrices satisfy an su(2) algebra and commute at different sites of the spin chain. On the contrary, fermionic operators at different sites anticommute. For this reason, to build a fermionic representation of su(2), one needs to include a highly non-local factor to satisfy the anticommutation relation. The solution for this problem was found by Jordan and Wigner in a seminal paper [119]. The Jordan-Wigner transformation is given by

$$
\begin{aligned}
Z_j &= -(\hat{f}_j^\dagger + \hat{f}_j) \prod_{m=1}^{j-1} (1 - 2\hat{f}_m^\dagger \hat{f}_m) \\
Y_j &= -\mathrm{i}(\hat{f}_j^\dagger - \hat{f}_j) \prod_{m=1}^{j-1} (1 - 2\hat{f}_m^\dagger \hat{f}_m) \\
X_j &= 1 - 2\hat{f}_j^\dagger \hat{f}_j .
\end{aligned}
\tag{E1}
$$

Here the operators $\hat{f}_j^\dagger$ and $\hat{f}_j$ are the fermionic creation and annihilation operators in real space, satisfying the anticommutation relations $\{\hat{f}_i, \hat{f}_j^\dagger\} = \delta_{i,j}$ and $\{\hat{f}_i, \hat{f}_j\} = \{\hat{f}_i^\dagger, \hat{f}_j^\dagger\} = 0$.

By using this transformation, the Hamiltonian in Eq. (24) becomes

$$
\begin{aligned}
\hat{\mathcal{H}} = &-\sum_{j=1}^N A_j (1 - 2\hat{f}_j^\dagger \hat{f}_j) - J \sum_{j=1}^{N-1} (\hat{f}_j^\dagger - \hat{f}_j)(\hat{f}_{j+1}^\dagger + \hat{f}_{j+1}) \\
&- \sum_{j=1}^N K_j (\hat{f}_j^\dagger + \hat{f}_j) \prod_{m=1}^{j-1} (1 - 2\hat{f}_m^\dagger \hat{f}_m) \\
&- J(\hat{f}_N^\dagger - \hat{f}_N)(\hat{f}_{N+1}^\dagger + \hat{f}_{N+1}) \prod_{m=1}^N (1 - 2\hat{f}_m^\dagger \hat{f}_m) .
\end{aligned}
\tag{E2}
$$

From this we can see that the disordered spin chain maps to a highly non-local Hamiltonian of interacting fermions. The last term of the Hamiltonian is nothing but the parity operator $\hat{\Pi} = \bigotimes_{j=1}^N X_j$ discussed in the main text. One can show that the boundary conditions of the fermions allow to map the Hamiltonian into two coupled blocks with different parities. This can be achieved by using the projector $\hat{Q}_\sigma = [\hat{1} + (-1)^\sigma \hat{\Pi}]/2$ into the subspaces with parity eigenvalue $(-1)^\sigma$ for $\sigma = 0, 1$, defined in the main text and the identity $\hat{Q}_0 + \hat{Q}_1 = \hat{1}$. The

Hamiltonian can be explicitly written as

$$(\hat{Q}_0 + \hat{Q}_1)\hat{\mathcal{H}}(\hat{Q}_0 + \hat{Q}_1) = \hat{\mathcal{H}}^{(+)} + \hat{\mathcal{H}}^{(-)} + \hat{\mathcal{H}}^{(+-)} . \quad \text{(E3)}$$

The positive and negative parity sector correspond to fermions with anti-periodic $\hat{f}_{N+1} = -\hat{f}_1$ and periodic $\hat{f}_{N+1} = \hat{f}_1$ boundary conditions, respectively [120, 121]. The two diagonal blocks of this decomposition can be written in terms of the integrable part of the Hamiltonians as follows

$$\hat{\mathcal{H}}^{(\pm)} = \hat{Q}_\sigma \left[ -\sum_{j=1}^N A_j(1 - 2\hat{f}_j^\dagger \hat{f}_j) \right] \hat{Q}_\sigma$$
$$+ \hat{Q}_\sigma \left[ -J\sum_{j=1}^N (\hat{f}_j^\dagger - \hat{f}_j)(\hat{f}_{j+1}^\dagger + \hat{f}_{j+1}) \right] \hat{Q}_\sigma . \quad \text{(E4)}$$

The longitudinal field term $\hat{\mathcal{H}}_L = -\sum_{j=1}^N K_j(\hat{f}_j^\dagger + \hat{f}_j)\prod_{m=1}^{j-1}(1 - 2\hat{f}_m^\dagger \hat{f}_m)$ in Eq. (E2) breaks the parity of the model and thus couples the different parity sectors giving rise to the term $\hat{\mathcal{H}}^{(+-)}$. In summary, the different parity sectors can be separated by taking into account the boundary conditions of the fermions, while the longitudinal field is responsible for the coupling between different irreps.

Next, let us explore how to decompose the Hamiltonian in terms of invariant subspaces under the group of spatial translations. To do that, we need to use the discrete Fourier transformation $\hat{f}_j = \frac{e^{-i\frac{\pi}{4}}}{\sqrt{N}}\sum_k \hat{F}_k e^{ikj}$ (see Ref. [120]) to the Ising model in the decomposition Eq. (E4), where $\hat{F}_k$ is the fermionic annihilation operator of momentum $k$ in the Fourier space. Of course, from our previous discussion on the relation between parity and boundary conditions, only discrete values of the momenta $k$ are allowed within a given parity sector [120]. We will denote these particular values as $k_\pm$.

Before doing the explicit calculation, we can see that the Ising interaction term $\hat{\mathcal{H}}_I = -J\sum_{j=1}^N (\hat{f}_j^\dagger - \hat{f}_j)(\hat{f}_{j+1}^\dagger + \hat{f}_{j+1})$ is invariant under spatial translations and it can be written in diagonal form as $\hat{\mathcal{H}}_I = \sum_k J(\hat{\gamma}_k^\dagger \hat{\gamma}_k - 1/2)$, where the operators $\hat{\gamma}_k = u_k \hat{F}_k^\dagger + v_k^* \hat{F}_{-k}$ define the total momentum operator $\hat{P} = \sum_k k\hat{\gamma}_k^\dagger \hat{\gamma}_k$. This is a conserved quantity of the Ising interaction in our Hamiltonian defining the symmetric sectors under translational invariance.

Both the transverse and longitudinal fields in our model break the translational symmetry and generate coupling between different sectors with momenta $k$. To see how the different sectors are coupled, it is enough to calculate the explicit form of the transverse field term $\hat{\mathcal{H}}_T = -\sum_{j=1}^N G_i(1 - 2\hat{f}_j^\dagger \hat{f}_j)$ in the momentum represen-

tation, as follows

$$\hat{\mathcal{H}}_T = -\sum_{j=1}^N G_i(1 - 2\hat{f}_j^\dagger \hat{f}_j) = -\sum_{j=1}^N G_i + 2\sum_{k,k'} M_{k,k'} \hat{F}_k^\dagger \hat{F}_{k'}$$
$$= -\sum_{j=1}^N G_i + \sum_{k,k'} (A_{k,k'} \hat{\gamma}_k^\dagger \hat{\gamma}_{k'} + B_{k,k'} \hat{\gamma}_k^\dagger \hat{\gamma}_{k'}^\dagger + C_{k,k'} \hat{\gamma}_k \hat{\gamma}_{k'}) .$$
$$\text{(E5)}$$

This expression already exhibits high complexity, as the disorder coupled the different momenta $k$ and while keeping a good parity. Further, the longitudinal term couples all the subspaces with momenta $k$ for different parities.

In summary, while we can use tools from condensed matter physics, the mapping to fermions makes the problem intractable. For this reason, our novel approach in this work is advantageous, as we work directly with the spin operators without using fermions.

## Appendix F: Harper model on a cylinder and quantum circuits

Our goal in this section is to demonstrate that by considering periodic boundary conditions, the Harper-Hofstadter model [67] can be represented using a simple quantum circuit, which simplifies the task of Hamiltonian simulation that is essential for quantum phase estimation.

To start with, we can directly perform a QFT on the register using the digital encoding $\boldsymbol{y}$ of the integer $y$ in the Harper model in Eq. (31). As the magnetic translations factorize

$$\hat{\mathcal{U}}_b = \left( \sum_{\boldsymbol{x}} |\boldsymbol{x}\rangle\langle\boldsymbol{x}+1| \right) \otimes \left( \sum_{\boldsymbol{y}} |\boldsymbol{y}\rangle\langle\boldsymbol{y}| \right)$$
$$\hat{\mathcal{V}}_b = \left( \sum_{\boldsymbol{x}} e^{2i\pi xb} |\boldsymbol{x}\rangle\langle\boldsymbol{x}| \right) \otimes \left( \sum_{\boldsymbol{y}} |\boldsymbol{y}\rangle\langle\boldsymbol{y}+1| \right) , \quad \text{(F1)}$$

we can perform QFT along the $y$ axis to obtain

$$U_{\text{QFT}}\hat{\mathcal{U}}_b U_{\text{QFT}}^\dagger = \sum_{\boldsymbol{k_y},\boldsymbol{x}} |\boldsymbol{x}\rangle\langle\boldsymbol{x}+1| \otimes |\boldsymbol{k_y}\rangle\langle\boldsymbol{k_y}|$$
$$U_{\text{QFT}}\hat{\mathcal{V}}_b U_{\text{QFT}}^\dagger = \sum_{\boldsymbol{k_y},\boldsymbol{x}} e^{2i\pi(xb-k_y/N)} |\boldsymbol{x}\rangle\langle\boldsymbol{x}| \otimes |\boldsymbol{k_y}\rangle\langle\boldsymbol{k_y}| .$$
$$\text{(F2)}$$

By using these identities, we can show that Eq. (31) transforms under $U_{\text{QFT}}$ as $U_{\text{QFT}}\hat{\mathcal{H}}U_{\text{QFT}}^\dagger = \sum_{k_y} \hat{\mathcal{H}}_{k_y} \otimes |\boldsymbol{k_y}\rangle\langle\boldsymbol{k_y}|$ with $\hat{\mathcal{H}}_{k_y}$ defined as

$$\hat{\mathcal{H}}_{k_y} = \sum_{\boldsymbol{x}} \left( J_x e^{2i\pi(xb-k_y/N)} |\boldsymbol{x}\rangle\langle\boldsymbol{x}| + J_y |\boldsymbol{x}\rangle\langle\boldsymbol{x}+1| + \text{H.c} \right) .$$
$$\text{(F3)}$$

By using the expressions discussed above, we can show that the evolution operator for the Harper-Hofstadter Hamiltonian can be written in terms of a control unitary, as follows

$$e^{-i\hat{\mathcal{H}}t} = U_{\mathrm{QFT}}^{\dagger} \left( \sum_{k_y} V_{k_y} \otimes |\boldsymbol{k_y}\rangle \langle \boldsymbol{k_y}| \right) U_{\mathrm{QFT}} \ , \quad \text{(F4)}$$

where $U_{\mathrm{QFT}}$ is acting on the second register. Thus, the evolution operator can be simplified using the irreps (momenta) $|\boldsymbol{k_y}\rangle$ and the unitary $V_{k_y} = e^{-\hat{\mathcal{H}}_{k_y}t}$.

[1] A. J. Buras, J. Ellis, M. K. Gaillard, and D. V. Nanopoulos, Nuclear Physics B **135**, 66 (1978).
[2] S. Weinberg, Rev. Mod. Phys. **52**, 515 (1980).
[3] R. Jozsa, Computing in Science & Engineering **3**, 34 (2001).
[4] C. Lomont, arXiv (2004), quant-ph/0411037 [quant-ph].
[5] S. M. Girvin and K. Yang, *Modern condensed matter physics* (Cambridge University Press, 2019).
[6] D. C. Harris and M. D. Bertolucci, *Symmetry and spectroscopy: an introduction to vibrational and electronic spectroscopy* (Courier Corporation, 1989).
[7] C. W. Curtis and I. Reiner, *Representation theory of finite groups and associative algebras*, Vol. 356 (American Mathematical Soc., 1966).
[8] R. Goodman, N. R. Wallach, *et al.*, *Symmetry, representations, and invariants*, Vol. 255 (Springer, 2009).
[9] P. Diaconis and D. Rockmore, Journal of the American Mathematical Society **3**, 297 (1990).
[10] D. K. Maslen, Journal of Fourier Analysis and Applications **4**, 19 (1998).
[11] A. Terras, *Fourier analysis on finite groups and applications*, 43 (Cambridge University Press, 1999).
[12] D. Rowe, M. Carvalho, and J. Repka, Reviews of Modern Physics **84**, 711 (2012).
[13] D. Rowe, J. Repka, and M. Carvalho, Journal of Mathematical Physics **52** (2011).
[14] R. Howe, Transactions of the American Mathematical Society **313**, 539 (1989).
[15] R. Howe, The Schur lectures (1992)(Tel Aviv) , 1 (1995).
[16] S. M. Goodlett, N. L. Kitzmiller, J. M. Turney, and H. F. Schaefer, The Journal of Chemical Physics **161** (2024).
[17] P. Kratzer and J. Neugebauer, Frontiers in chemistry **7**, 106 (2019).
[18] R. McWeeny, B. Sutcliffe, and G. Brink, Physics Today **24**, 50 (1971).
[19] W. Pauli, Phys. Rev. **58**, 716 (1940).
[20] A. I. Krylov, Annu. Rev. Phys. Chem. **59**, 433 (2008).
[21] M. Nooijen and R. J. Bartlett, The Journal of chemical physics **104**, 2652 (1996).
[22] J. Paldus, in *The Unitary Group for the evaluation of electronic energy matrix elements* (Springer, 1981) pp. 1–50.
[23] X. Li and J. Paldus, Theoretical Chemistry Accounts **133**, 1 (2014).
[24] V. Sonnad, J. Escher, M. Kruse, and R. Baker, *An informal overview of the unitary group approach*, Tech. Rep. (Lawrence Livermore National Lab.(LLNL), Livermore, CA (United States), 2016).
[25] J. Hinze, *The Unitary Group for the Evaluation of Electronic Energy Matrix Elements: Unitary Group Workshop 1979*, Vol. 22 (Springer Science & Business Media, 2012).
[26] F. A. Matsen and R. Pauncz, Studies in physical and theoretical chemistry **44** (1986).
[27] I. Shavitt, in *The Unitary Group for the Evaluation of Electronic Energy Matrix Elements* (Springer, 1981) pp. 51–99.
[28] P. Hoyer, arXiv preprint quant-ph/9702028 (1997).
[29] R. Beals, in *Proceedings of the twenty-ninth annual ACM symposium on Theory of computing* (1997) pp. 48–53.
[30] D. Bacon, I. L. Chuang, and A. W. Harrow, Phys. Rev. Lett. **97**, 170502 (2006).
[31] H. Krovi, Quantum **3**, 122 (2019).
[32] A. W. Harrow, arXiv preprint quant-ph/0512255 (2005).
[33] A. M. Childs and W. van Dam, Rev. Mod. Phys. **82**, 1 (2010).
[34] D. Grinko, A. Burchardt, and M. Ozols, arXiv preprint arXiv:2310.02252 (2023).
[35] Q. T. Nguyen, arXiv preprint arXiv:2310.01613 (2023).
[36] J. Fei, S. Timmerman, and P. Hayden, arXiv preprint arXiv:2310.01637 (2023).
[37] M. L. LaBorde, S. Rethinasamy, and M. M. Wilde, arXiv preprint arXiv:2407.17563 (2024).
[38] M. L. LaBorde, S. Rethinasamy, and M. M. Wilde, Quantum **7**, 1120 (2023).
[39] M. L. LaBorde and M. M. Wilde, Phys. Rev. Lett. **129**, 160503 (2022).
[40] J. J. Meyer, M. Mularski, E. Gil-Fuster, A. A. Mele, F. Arzani, A. Wilms, and J. Eisert, PRX Quantum **4**, 010328 (2023).
[41] C. Lyu, X. Xu, M.-H. Yung, and A. Bayat, Quantum **7**, 899 (2023).
[42] M. C. Tran, Y. Su, D. Carney, and J. M. Taylor, PRX Quantum **2**, 010323 (2021).
[43] N. H. Nguyen, M. C. Tran, Y. Zhu, A. M. Green, C. H. Alderete, Z. Davoudi, and N. M. Linke, PRX Quantum **3**, 020324 (2022).
[44] H. Zhao, M. Bukov, M. Heyl, and R. Moessner, PRX Quantum **4**, 030319 (2023).
[45] J. Heredge, M. West, L. Hollenberg, and M. Sevior, "Non-unitary quantum machine learning," (2024), arXiv:2405.17388 [quant-ph].
[46] J. M. Martyn, Z. M. Rossi, A. K. Tan, and I. L. Chuang, PRX quantum **2**, 040203 (2021).
[47] A. Gilyén, Y. Su, G. H. Low, and N. Wiebe, in *Proceedings of the 51st Annual ACM SIGACT Symposium on Theory of Computing* (2019) pp. 193–204.
[48] G. H. Low and I. L. Chuang, Physical review letters

**118**, 010501 (2017).

[49] W. Fulton and J. Harris, "Representations of finite groups," in *Representation Theory: A First Course* (Springer New York, New York, NY, 2004) pp. 3–11.

[50] R. Gilmore and J. Katriel, Journal of Physics A: Mathematical and General **25**, 2253 (1992).

[51] M. Rosenkranz, E. Brunner, G. Marin-Sanchez, N. Fitzpatrick, S. Dilkes, Y. Tang, Y. Kikuchi, and M. Benedetti, "Quantum state preparation for multivariate functions," (2024), arXiv:2405.21058 [quant-ph].

[52] T. Khattar and C. Gidney, "Rise of conditionally clean ancillae for optimizing quantum circuits," (2024), arXiv:2407.17966 [quant-ph].

[53] C. Gidney, Quantum **2**, 74 (2018).

[54] O. Bratteli, Transactions of the American Mathematical Society **171**, 195 (1972).

[55] Y. Kawano and H. Sekigawa, Journal of Symbolic Computation **75**, 219 (2016).

[56] R. R. Holmes, "A recursion formula for the irreducible characters of the symmetric group," (2017), arXiv:1712.08023 [math.GR].

[57] M. L. LaBorde, S. Rethinasamy, and M. M. Wilde, "Quantum algorithms for realizing symmetric, asymmetric, and antisymmetric projectors," (2024), arXiv:2407.17563 [quant-ph].

[58] T. N. Georges, B. K. Berntson, C. Sünderhauf, and A. V. Ivanov, "Pauli decomposition via the fast walsh-hadamard transform," (2024), arXiv:2408.06206 [quant-ph].

[59] A. M. Childs and N. Wiebe, Quantum Information and Computation **12**, 901 (2012).

[60] R. Babbush, C. Gidney, D. W. Berry, N. Wiebe, J. McClean, A. Paler, A. Fowler, and H. Neven, Phys. Rev. X **8**, 041015 (2018).

[61] T. Pető, F. Iglói, and I. A. Kovács, arXiv preprint arXiv:2210.09380 (2022).

[62] R. Berkovits, Phys. Rev. B **105**, 104203 (2022).

[63] J. D. Noh, Phys. Rev. E **104**, 034112 (2021).

[64] G. Vionnet, B. Kumar, and F. Mila, Phys. Rev. B **95**, 174404 (2017).

[65] C. Peng and X. Cui, Phys. Rev. B **106**, 214311 (2022).

[66] R. Coldea, D. Tennant, E. Wheeler, E. Wawrzynska, D. Prabhakaran, M. Telling, K. Habicht, P. Smeibidl, and K. Kiefer, Science **327**, 177 (2010).

[67] D. R. Hofstadter, Phys. Rev. B **14**, 2239 (1976).

[68] A. Connes, *Noncommutative geometry* (Springer, 1994).

[69] P. Roushan, C. Neill, J. Tangpanitanon, V. M. Bastidas, A. Megrant, R. Barends, Y. Chen, Z. Chen, B. Chiaro, A. Dunsworth, *et al.*, Science **358**, 1175 (2017).

[70] J. Puig, Communications in mathematical physics **244**, 297 (2004).

[71] M. Sajid, J. K. Asbóth, D. Meschede, R. F. Werner, and A. Alberti, Phys. Rev. B **99**, 214303 (2019).

[72] A. Javadi-Abhari, M. Treinish, K. Krsulich, C. J. Wood, J. Lishman, J. Gacon, S. Martiel, P. D. Nation, L. S. Bishop, A. W. Cross, B. R. Johnson, and J. M. Gambetta, "Quantum computing with Qiskit," (2024), arXiv:2405.08810 [quant-ph].

[73] R. P. Feynman, in *Feynman and computation* (cRc Press, 2018) pp. 133–153.

[74] P. R. Bunker and P. Jensen, *Molecular symmetry and spectroscopy*, Vol. 46853 (NRC research press, 2006).

[75] J. T. Iosue, K. Sharma, M. J. Gullans, and V. V. Albert, Phys. Rev. X **14**, 011013 (2024).

[76] C. Dankert, R. Cleve, J. Emerson, and E. Livine, Phys. Rev. A **80**, 012304 (2009).

[77] B. Nagy and F. Jensen, Reviews in computational chemistry **30**, 93 (2017).

[78] T. Chowdhury, E. C. Sadler, and T. J. Kempa, Chemical reviews **120**, 12563 (2020).

[79] S. Koseki, N. Matsunaga, T. Asada, M. W. Schmidt, and M. S. Gordon, The Journal of Physical Chemistry A **123**, 2325 (2019).

[80] T. Zhang, S. Banerjee, L. N. Koulias, E. F. Valeev, A. E. DePrince III, and X. Li, The Journal of Physical Chemistry A **128**, 3408 (2024).

[81] W. Liu, Molecular Physics **108**, 1679 (2010).

[82] Y. Y. Atas, J. F. Haase, J. Zhang, V. Wei, S. M.-L. Pfaendler, R. Lewis, and C. A. Muschik, Phys. Rev. Res. **5**, 033184 (2023).

[83] E. A. Martinez, C. A. Muschik, P. Schindler, D. Nigg, A. Erhard, M. Heyl, P. Hauke, M. Dalmonte, T. Monz, P. Zoller, *et al.*, Nature **534**, 516 (2016).

[84] H. L. Stormer, Rev. Mod. Phys. **71**, 875 (1999).

[85] J. K. Jain, Phys. Rev. B **41**, 7653 (1990).

[86] Y. Hatsugai, M. Kohmoto, and Y.-S. Wu, Phys. Rev. B **43**, 2661 (1991).

[87] A. H. Castro Neto, F. Guinea, N. M. R. Peres, K. S. Novoselov, and A. K. Geim, Rev. Mod. Phys. **81**, 109 (2009).

[88] E. Fradkin, *Quantum field theory: an integrated approach* (Princeton University Press, 2021).

[89] M. B. Halpern, Phys. Rev. D **12**, 1684 (1975).

[90] W. J. Chetcuti, T. Haug, L.-C. Kwek, and L. Amico, SciPost Physics **12**, 033 (2022).

[91] M. A. Cazalilla, A. Ho, and M. Ueda, New Journal of Physics **11**, 103033 (2009).

[92] X. Zhang, M. Bishof, S. L. Bromley, C. V. Kraus, M. S. Safronova, P. Zoller, A. M. Rey, and J. Ye, science **345**, 1467 (2014).

[93] A. V. Gorshkov, M. Hermele, V. Gurarie, C. Xu, P. S. Julienne, J. Ye, P. Zoller, E. Demler, M. D. Lukin, and A. Rey, Nature physics **6**, 289 (2010).

[94] G. R. Stewart, Rev. Mod. Phys. **56**, 755 (1984).

[95] X.-J. Yu, S.-H. Shi, L. Xu, and Z.-X. Li, Phys. Rev. Lett. **132**, 036704 (2024).

[96] Y. Liu, S. Singh, K. C. Smith, E. Crane, J. M. Martyn, A. Eickbusch, A. Schuckert, R. D. Li, J. Sinanan-Singh, M. B. Soley, *et al.*, arXiv preprint arXiv:2407.10381 (2024).

[97] W. Cai, Y. Ma, W. Wang, C.-L. Zou, and L. Sun, Fundamental Research **1**, 50 (2021).

[98] V. V. Albert, K. Noh, K. Duivenvoorden, D. J. Young, R. Brierley, P. Reinhold, C. Vuillot, L. Li, C. Shen, S. M. Girvin, *et al.*, Physical Review A **97**, 032346 (2018).

[99] S. Girvin, arXiv preprint arXiv:1710.03179 (2017).

[100] A. L. Grimsmo and S. Puri, PRX Quantum **2**, 020101 (2021).

[101] R. Babbush, D. W. Berry, R. Kothari, R. D. Somma, and N. Wiebe, Phys. Rev. X **13**, 041041 (2023).

[102] S. Lee, J. Lee, H. Zhai, Y. Tong, A. M. Dalzell, A. Kumar, P. Helms, J. Gray, Z.-H. Cui, W. Liu, *et al.*, Nature communications **14**, 1952 (2023).

[103] I. M. Georgescu, S. Ashhab, and F. Nori, Rev. Mod. Phys. **86**, 153 (2014).

[104] A. J. Daley, I. Bloch, C. Kokail, S. Flannigan, N. Pearson, M. Troyer, and P. Zoller, Nature **607**, 667 (2022).

[105] J. Bermejo-Vega, D. Hangleiter, M. Schwarz, R. Raussendorf, and J. Eisert, Phys. Rev. X **8**, 021010 (2018).

[106] G. K.-L. Chan, Faraday Discussions (2024).

[107] N. J. Ward, I. Kassal, and A. Aspuru-Guzik, The Journal of chemical physics **130** (2009).

[108] X.-K. Song, F.-G. Deng, L. Lamata, and J. G. Muga, Phys. Rev. A **95**, 022332 (2017).

[109] C. F. Kane, N. Gomes, and M. Kreshchuk, Phys. Rev. A **110**, 012455 (2024).

[110] T.-C. Yen, A. Ganeshram, and A. F. Izmaylov, npj Quantum Information **9**, 14 (2023).

[111] T.-C. Yen and A. F. Izmaylov, PRX Quantum **2**, 040320 (2021).

[112] H.-Y. Huang, R. Kueng, and J. Preskill, Nature Physics **16**, 1050 (2020).

[113] H. H. S. Chan, R. Meister, T. Jones, D. P. Tew, and S. C. Benjamin, Science Advances **9**, eabo7484 (2023).

[114] R. J. Harrison, G. I. Fann, T. Yanai, Z. Gan, and G. Beylkin, The Journal of chemical physics **121**, 11587 (2004).

[115] L. Piela, *Ideas of quantum chemistry* (Elsevier, 2006).

[116] A. K. Tan, Y. Liu, M. C. Tran, and I. L. Chuang, Phys. Rev. A **107**, 042429 (2023).

[117] A. Coleman (Academic Press, 1968) pp. 83–108.

[118] C. Moore, D. Rockmore, and A. Russell, ACM Transactions on Algorithms (TALG) **2**, 707 (2006).

[119] P. Jordan and E. P. Wigner, Z. Phys **47**, 14 (1928).

[120] J. Dziarmaga, Phys. Rev. Lett. **95**, 245701 (2005).

[121] M. Vogl, G. Schaller, and T. Brandes, Phys. Rev. Lett. **109**, 240402 (2012).